Healthy Climate and Energy Savings: Using Thermal Ceramic Panels and Solar Thermal Panels in Mediterranean Housing Blocks

Víctor Echarri-Iribarren [1,*], Carlos Rizo-Maestre [1] and Fernando Echarri-Iribarren [2]

[1] Department of Building Construction, University of Alicante, 03690 Alicante, Spain; carlosrm@ua.es
[2] Department of Environmental Biology, University of Navarra, 31009 Pamplona, Spain; fecharri@unav.es
* Correspondence: Victor.Echarri@ua.es; Tel.: +34-965-903677

check for updates

Abstract: Radiant surface conditioning systems based on capillary tube mats not only provide high standards of comfort, but they also generate substantial energy savings. These systems allow for using renewable energies such as solar thermal panels because they function with water at moderate temperatures—lower in winter and higher in summer—compared to fan-coil systems or hot water radiator systems. Moreover, in summer, they can be combined with solar cooling systems based on lithium chloride or absorption systems based on lithium bromide, which enable the cooling of water at 15–16 °C by means of solar thermal panel energy collection. This further reduces the annual energy. The purpose of this study was to examine the application of thermal ceramic panels (TCP) containing prolipropylen (PPR) capillary tube mats, in residential buildings in the Spanish Mediterranean. The water distribution system was set up individually from a heat pump and was combined with a community system of solar thermal panels. After monitoring a home over a complete one-year cycle, the annual energy demand was quantified through simulations, based on both the radiant system and the VRV system, as well as in combination with a thermal solar panel system. TCP panels reduced the annual energy demands by 31.48%, and the additional investment cost of €11,497 could be amortized over 23.31 years. The combination of TCP panels with 18.5 m^2 of solar thermal panels reduced the annual energy demand by 69.47%, and the investment of €20,534 of additional cost could be amortized over 15.67 years. The energy consumptions of installation elements were also comparatively quantified.

Keywords: thermal ceramic panel; capillary tube systems; energy saving; renewable energy; solar refrigeration technology

1. Introduction

It is well known that building usage represents around 40% of the final energy consumption in the European Union (EU) [1,2] and that substantial environmental impacts are generated by building construction [3], use, maintenance, and because of the Construction and Demolition Waste (CWD). Buildings' facade enclosures undeniably constitute a major subject of research within the field of energy consumption [4,5]. Air permeability, construction quality, vapour permeability, or thermal bridges due to discontinuities in thermal insulation materials all play an important role [6]. Moreover, heat transfer affects comfort levels demanded by users [7,8] and a certain amount of energy consumption is needed to achieve these comfort levels in buildings [9,10].

Air conditioning systems must be able to provide these conditions of comfort. Convective systems modify the conditions of temperature and the specific humidity of indoor air, counteracting thermal loads. Radiant surface systems work mainly through energy radiation exchanges with users, significantly increasing the comfort standards.

Quality standards of housing constructions in the Spanish Mediterranean have been inferior to that of other Spanish regions and many EU countries. Regulations applied in Spain over the 1970s–1990s were very undemanding concerning parameters such as thermal transmittance, the air permeability in frameworks and joinery, thermal bridge reductions in enclosures, etc. In recent years, the Technical Building Code (CTE, or Código Técnico de la Edificación) has led to the requirement of higher construction standards in Spain. The technical report DB-HE on energy saving [11] envisages the use of the unified tool Lider-Calener (HULC) [12] for both single-family and collective housing projects. The tool includes a project model and a climatic file adjusted to the building's location and altitude. Annual energy demand values, as well as energy ratings, can be obtained based on the air conditioning systems and energy sources used in the building. Other tools such as Design Builder or TRNSYS allow us to make adjustments according to actual use, for example, window opening and closing time slots, bioclimatic techniques, or the use of enclosures' thermal inertia for thermal comfort and energy demand reduction through phase change materials [13].

In the Spanish Mediterranean, hot summer climatic conditions have led to air conditioning being installed in practically all modern buildings [5]. The most frequent system used in households is the convection VRV split system, with winter cycle inversion or a heat pump. Winter conditions are relatively favourable to users, so by installing high-quality envelopes, energy demand peaks at low temperatures can be easily met by the sporadic use of electric radiators, or air impulsion in the heat pump systems, all based on electric power.

In contrast to convective air conditioning systems, radiant surface conditioning systems have been used in buildings for decades. These systems use water or hydronics to carry out energy exchanges and have proven to be more energy efficient and have a shorter amortization period than those that use Joule effect electric energy [14]. Hydronic radiant surface conditioning systems (HRSC) use water at moderate temperatures between 29–35 °C in winter, and 15–17 °C in summer, allowing for the use of alternative energies, such as solar energy, geothermal energy, or chemical energy systems based on lithium chloride [15]. As a result, they generate significant energy savings due to energy collection sources as well as their water distribution efficiency through small electric circulators. Energy distribution via supply air requires a much higher consumption in split VRV systems than in hydronic systems [16]. In addition, these HRSC systems can be conditioned throughout the annual cycle, distributing cold or hot water as required. Despite a lack of energy policy, building planning, and tax exemption incentives, these air conditioning systems are starting to be implemented as people seek greater comfort, energy savings, and a reduction of environmental impacts.

In architecture, the first systems to distribute water through closed circuits used pipes made of copper or plastic (mainly reticulated polyethylene). The most common installation choice was radiant floor heating, and the systems were denominated "thick tube" systems. The usual diameters were 16 and 20 mm, with separations or "modules" of 10 cm to 30 cm. In the mid-1980s, thin tube or "capillary tube" systems were implemented, made of both copper and PPR [17]. The systems are mat-like, based on PPR tubes of around 3 mm in diameter. These mats were designed with gaps of around 8–10 mm between the tubes, which were attached to the flow, and return manifold tubes that were around 20 mm in diameter, by thermal fusion bonding. There are many ways of making the mats depending on the manifold tube layouts. The size of the gaps in the mat grid is variable, with widths from 150 mm to 1210 mm and lengths from 600 mm to 6000 mm. In this way, by hugely increasing the total surface area of the capillary tube walls and creating a high density of thin tubes, the energy exchange with the surface materials intended to be cooled or heated became more efficient. Furthermore, the ease of design, layout, and assembly of these capillary tube mat installations made it possible to apply them to floors, ceilings, and walls in any geometrical shape. The distribution circuits are managed from a substation that includes a forward manifold with thermostatic control valves, and a return manifold with balancing valves. A plate exchanger properly regulates the temperature of the water distributed to the circuits. Table 1 shows a comparison of the technical characteristics between PPR capillary tubes and thick cross-linked polyethylene tubes (PER).

Table 1. The comparison between 20 mm diameter cross-linked polyethylene tubes and capillary tubes, for a cold emission of 70 W/m^2 with a 1 m wide and 2 m or 4 m long panel.
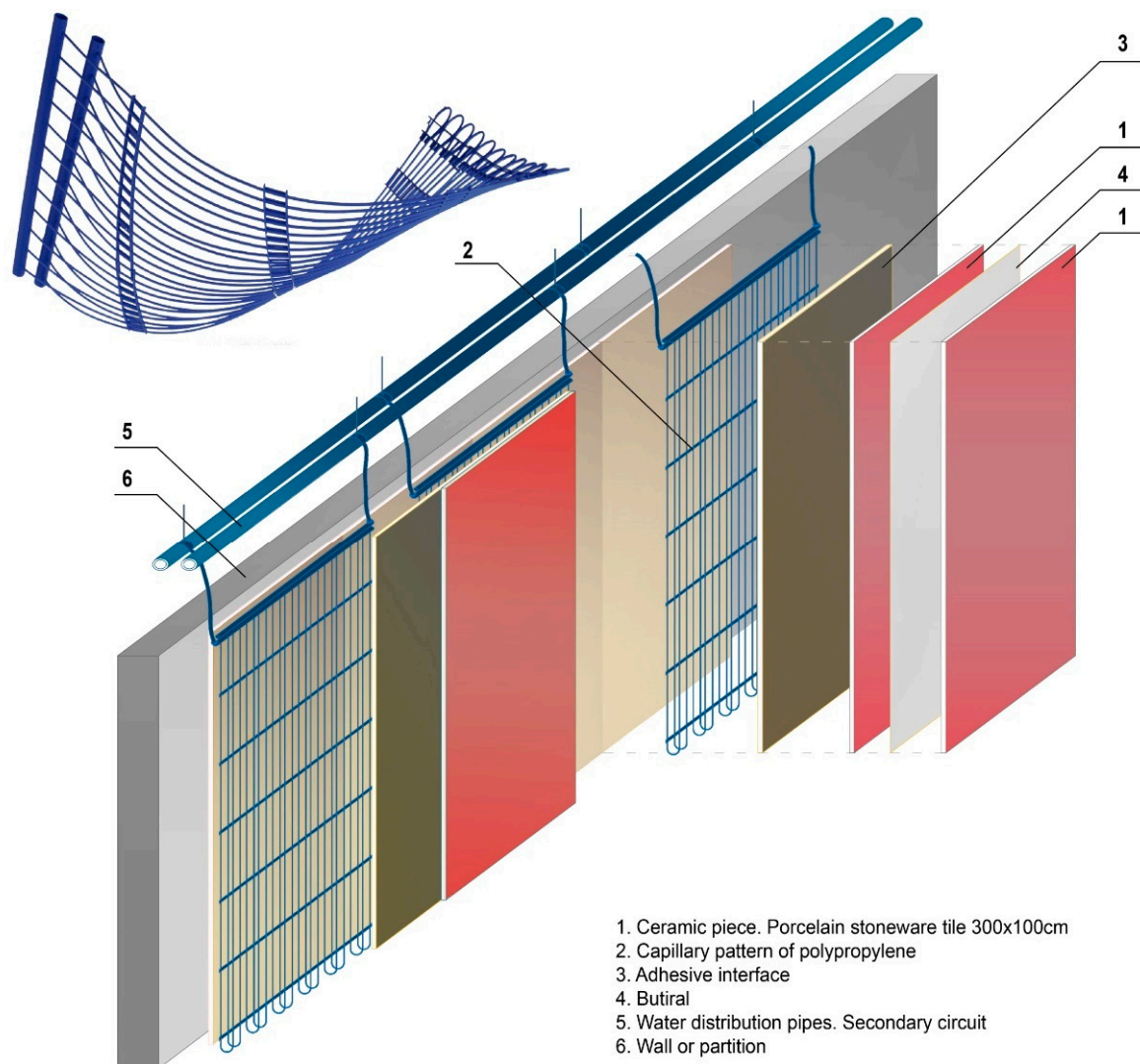
	PPR Capillary Tube Mats		Thick PER Tubes	
Tube diameter, mm	3.4		20	
Gap between tubes, mm	10		150	
Thickness of tubes, mm	0.55		2	
Water content, l/m^2	0.39		1.70	
Mat length, m	2	4	2	4
Water flow $\Delta T = 3\,°C$	40	80	40	80
Load los, mH$_2$O	0.2	0.55	0.03	0.12
Water speed, m/s	0.27	0.53	0.06	0.13
No. of Reynolds	540	1080	910	1820

Today, most common installation systems are underfloor, in plaster or metal modular suspended false ceilings, or in plasterboard cladding in walls and ceilings [18]. A new way of conditioning architectural spaces offering remarkable advantages in terms of comfort and energy saving was, thus, achieved [19]: it became possible to heat and cool via the very surfaces of the area spaces themselves. It is also possible to make prefabricated panels with different finishing materials [20], which are connected to the round-trip water distribution circuits using a simple "click and cool" joint. The finishing material's thermal conductivity has an impact on the system's efficiency: the greater the conductivity, the higher the starting up speed and the greater the panels' thermal performance [21].

Compared to other air conditioning systems, few studies have been conducted on conditioning systems using PPR capillary tube mats in buildings. Most works have focused on ceilings and office use. Stetiu et al. obtained significant energy savings of 30% to 35% when they applied capillary tube mats to ceilings in commercial use and office building contexts [16]. Recently, Mikeska and Svendsen carried out research using integrated systems in concrete walls [22,23]. In addition to achieving high standards of comfort, they demonstrated that by simply lowering the water distribution temperature by 4 °C below the T_o, it was feasible to use groundwater or seawater as renewable energy sources, with significant energy savings. Imanari et al. obtained notable results from radiant ceilings in Japan, with energy savings between 10% and 17% [24]. Tye and Gosselin compared radiant systems in walls and ceilings in Canada, concluding that energy consumption differences could reach up to 6% depending on the location of the capillary tube mats in the architectural space [25]. Finally, Rhee and Kim reviewed the last 50 years of research [26]. They found that more attention was given to elaborating estimation methods and mathematical simulation models [27], as well as to evaluating thermal behaviour and energy savings, than to application system innovations [28,29].

Little research, however, has addressed housing, and less still on housing blocks. In addition, research on prefabricated wall panels and the use of renewable energies such as solar energy, especially in summer based on chemical energy systems (LiCl), is non-existent. This research takes into account the results of previous studies on single-family housing and offices on Spain's Mediterranean coast and thus inaugurates this line of research [30,31].

The "Technology and Sustainability in Architecture" research group at the University of Alicante (Spain), recently obtained a patent for a thermal ceramic panel (TCP) [32] based on large porcelain stoneware tiles that incorporate capillary tube mats made of polypropylene tubes using conductive paste adhesive (Beka, V.WLP.1 Thermal Conductive Paste) (Figure 1). The maximum format is 320 cm × 160 cm and 16 mm thick, with two large format ceramic tiles 3 mm thick, with a maximum weight of 22 kg/m^2, although the tiles can come in a single 3 mm or 9 mm thick piece weighing 12 kg/m^2 and 25 kg/m^2, respectively. This lightweight panel can be easily placed on walls and ceilings using a metal rail fixation system [33].

1. Ceramic piece. Porcelain stoneware tile 300x100cm
2. Capillary pattern of polypropylene
3. Adhesive interface
4. Butiral
5. Water distribution pipes. Secondary circuit
6. Wall or partition

Figure 1. Patent application No. P201001626. Ceramic Thermal Conditioning Panel.

In this article, we start with a technical presentation of radiant surface conditioning systems using hydronic systems based on PPR capillary tube mats, and their applications in buildings. We then describe the Thermal Ceramic Panel (TCP) conditioning patent for application to wall cladding and emphasize the scarce amount of research carried out so far in this field. The technical aspects that enable these systems to offer significant levels of comfort and energy consumption reductions are described below. Given the advantages of incorporating renewable energies—such as solar energy—into the system, we detail the technical characteristics of absorption, adsorption and cooling systems by means of a chemical energy system (LiCl). These systems could introduce hot or cold water at moderate temperatures into the air conditioning system. We then present a case study of the application of TCP panels to a housing block in the city of Alicante. A comparison is made with the air conditioning systems usually used in the region, i.e., convective VRV split systems. After examining the comfort levels, we assessed annual energy demand by simulating three scenarios or options (OP) using the Design Builder program. The costs of installation, the period of amortization of the investments, the reductions of CO_2 emissions, etc., were also evaluated. The main results can be found in Section 8.

2. Method

The methodology used in the study took into account the maintenance of indoor thermal comfort conditions based on the concept of operating temperature T_o and relative humidity values (RH) of 50%. In order to evaluate comfort, the user's energy loss values are taken into account [30], obtained from the following equations:

$$\sum q = q_{met} - q_{ev} \pm q_{ci} \pm q_{cvi} \pm q_{rdi} = 0 \tag{1}$$

where Σq was the body heat balance, q_{met} was the heat due to metabolic activity, q_{ev} was the heat given by evaporation (breathing and sweating), q_{ci} was the heat transferred or acquired by driving, q_{cvi} was the heat given or acquired by convection, and q_{rdi} was the heat given or acquired by radiation.

$$q_{cvi} = h_c(T_p - T_a) \tag{2}$$

where q_{cvi} was the convective heat flow per m^2 of the body's surface, h_c was the heat transfer coefficient, T_p was the surface temperature of the wall, and T_a was the ambient air temperature.

$$h_c = 8.3 \cdot v^{0.24} \left(W/m^{2\circ}C \right) \tag{3}$$

To calculate the radiation losses, Fanger's method was followed, quantifying the form factors that affect the determination of the real value of the average radiant wall temperatures [8]. The expression of the T_{rm} calculation can be simplified according to the expression collected in his manual:

$$T_{rm} = T_1 \cdot F_{P-1} + T_2 \cdot F_{P-2} + \cdots + T_N \cdot F_{P-N} \tag{4}$$

Experimentally, for areas with a usual size, between 20 and 30 m^2, and an approximate height of 2.6 m to 3 m, the form factors of the floor to ceiling and the wall to floor or ceiling are respectively around 0.4 and 0.15 [8,34].

$$T_{rm} = \frac{T_s + 0.15 \cdot \left(T_{p1} + T_{p2} + T_{p3} + T_{p4} \right) + 0.4 \cdot T_t}{2} \tag{5}$$

$$q_{rdi} = h_r(T_r - T_{rm}) \tag{6}$$

The hr coefficient of radiation losses adopted approximate values of 4.7 W/m$^2{}^{\circ}$C based on a human body's estimated temperature of 30 °C. Finally, the value of the operating temperature T_o:

$$T_o = \frac{h_r T_{rm} + h_c T_a}{h_r + h_c} \tag{7}$$

A dwelling included in a block of flats located near the Alicante city coast, on Benito Pérez Galdós Street, was monitored during the complete 2015 cycle. Surface temperature sensors (PT 100) were fixed on all the interior layers of the enclosure. The system used to pierce the layers produced a perforation of approximately 0.40 m in diameter in the lower right section. The sensors were thus introduced into all 5 layers that made up the wall. Subsequently, these layers were sealed back with similar materials to the original ones. The sensors enabled the drawing of a graph of thermal gradient curves throughout the year, as well as variations in the dynamic regime [35]. Wall surface temperatures, solar radiation, relative humidity, etc., could also be graphed. Simulations of the building's thermal and energy behaviour were carried out using the Design Builder tool. To calibrate the model, the house's monitoring results were used [35]. An office using TCP panels at the University of Alicante was also monitored, its performance was checked, and the parameters obtained from the surface temperature, the temperature and relative humidity of indoor air, the indoor air velocity, and convection currents were applied. The results obtained in previous studies on a single-family home next to the building, which also had TCP panels and had been monitored, were equally retrieved [30]. The home's electrical

energy consumption in its current state, measured with a conventional meter, also contributed to the model's calibration process. It was possible to make a comparative analysis with the single-family flat, but not with other building blocks, as this was the first time these TCP panels were implemented in these types of buildings. The implementation of capillary tube systems in housing blocks in the Spanish Mediterranean have not been researched either, until now [36].

This study aims at quantifying the annual energy demand reductions in multi-storey residential buildings on the Spanish Levante coast thanks to the use of thermal TCP panels, comparing it to that of conventional convective systems such as VRV and all-air installations. To perform the study, we installed a water distribution system based on the TCP panel capillary mat system (Figure 2). A domotic system for controlling the panel surface temperature parameters, indoor air temperature, and 50% of relative humidity was included. In addition, the extent of use of renewable energies in the TCP panel system was evaluated by incorporating thermal solar panels located on the common building roof into the system. To finish, we quantified the energy consumption of both systems for each component [37]: pumps, circulators, heat pumps, split ventilators, solar energy input from common roof panels, etc. Comparative tables were drawn up to show the energy saving results of TCP panel systems, especially when solar thermal panels were used in climatic areas with long periods of sunlight, both in summer and winter. Figure 3 shows the study's methodology flow diagram.

(**a**)   (**b**)

Figure 2. A thermal ceramic panel (TCP) in an office at Alicante University. (**a**) Distribution management substation. TCP panels in the standard office of the Multipurpose III building. University of Alicante; (**b**) Substation for management and control of distribution circuits.
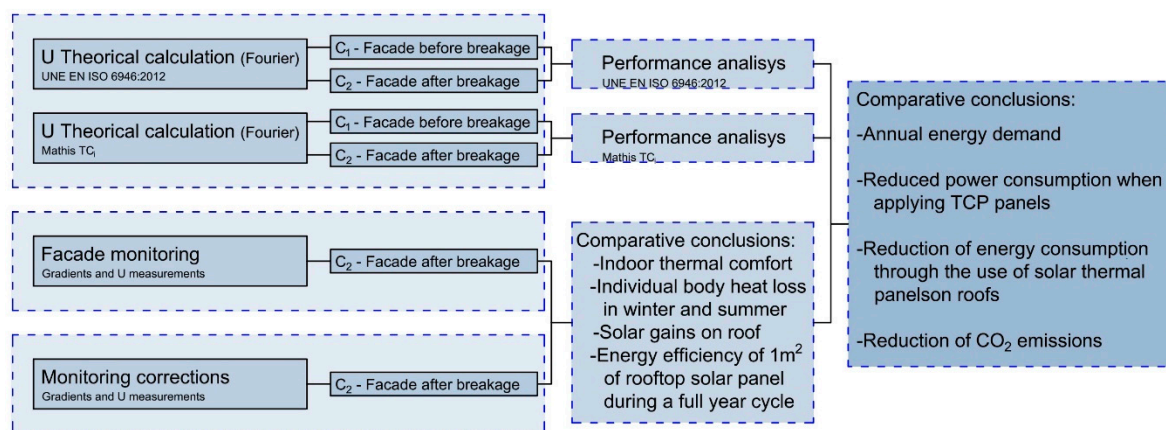
Figure 3. The flow diagram of the methodology followed in the study.

3. Energy Savings Compared to Other Air Conditioning Systems

Previous studies and publications have found that radiant systems lead to energy consumption reductions of between 20% and 30% compared to all-air systems [14,16]. In some cases, energy consumption savings can reach 40% when applying capillary tube solutions, compared to variable air volume systems [38]. However, research on residential use is still scarce, particularly in coastal climates, where energy consumption due to dehumidification can be high.

3.1. Water as a Means of Energy Transport

If we analyse the energy transport in air conditioning systems, from production to the points of diffusion, the required transport volumes are approximately 1000 times higher with air than with water. This is because the specific heat of water is four times higher than that of air, and the water density at 25 °C is 1000 kg/m^3 while that of air is 1.19 kg/m^3. Consequently, the electrical energy needed to run motors and fans in a forced air system is 80% higher than would be necessary with a radiant system [39].

This is one of the major reasons why the distribution of water at such moderate temperatures in buildings leads to high energy efficiency. In addition, if we evaluate the cold mode functioning, where the supply temperature is limited to dew point, not only do we achieve energy savings compared to other forced air, radiant and convective systems, but we also obtain powers of 75–90 W/m^2 in cooling mode, unattainable by other radiant systems.

3.2. The Decrease in Thermal Load Peaks

Radiant systems based on PPR capillary tubes are active solutions. Not only do they act on the air in the room, but on all the premises' enclosures, modifying their temperature via the walls' radiating action. Thermal loads by heat transmission through enclosures according to Fourier's law are significantly reduced by decreasing the thermal gap between the indoor and outdoor air temperatures. In summer, indoor air can be 3 °C warmer than in forced air systems, with a reduction in these thermal loads of around 25% [16]. A similar process occurs in winter since the temperature is lower than in convective and forced air systems. This entails a drop in thermal load peaks that cause the peak demands to be absorbed and their value reduced compared to "all-air" systems. These values can vary depending on the type of location, climate, etc. The range in the peak loads varies between 20% and 40% [40].

3.3. Thermal Performance of the Installation

The water temperatures needed for use in the capillary mats are very moderate (about 15 °C in the cold mode and 35 °C in the heat mode). This improves the performance of the production source compared to other systems [15]. If the chosen source is a heat pump (aerothermal or geothermal),

a lower energy consumption will be achieved since heat pumps improve the machine's COP by supplying water at more moderate temperatures [41,42]. The installation's overall performance can also be increased by taking advantage of alternative or renewable energies [43,44], such as solar or geothermal energy (Figure 4) [45].
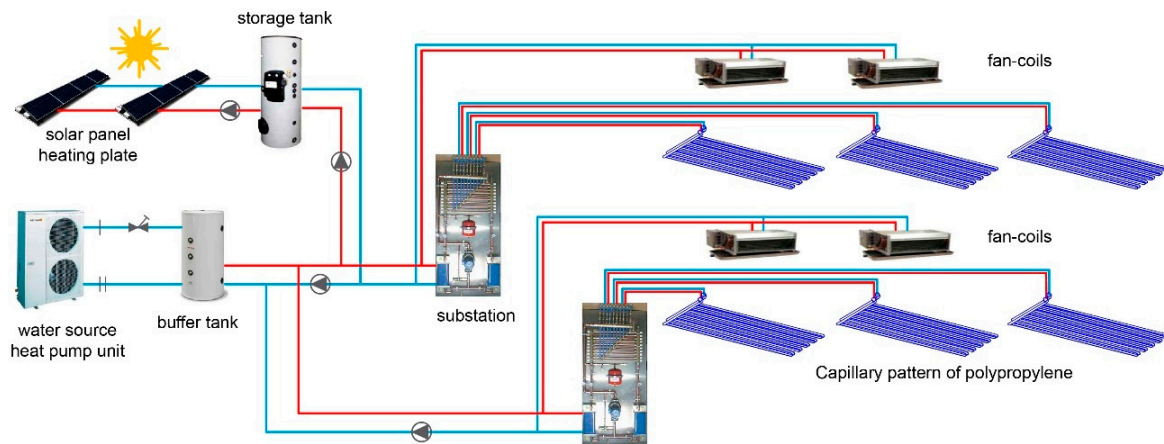
Figure 4. The circuit installation diagram based on two tubes with substations and renewable energies.

4. Solar Energy Use in the Installation. Absorption, Chemical Energy, and Adsorption Systems

The energy efficiency of the capillary tube hydronic system and environmental impact reductions are all enhanced by its ability to work with water at moderate temperatures. Conventional heating and cooling systems require higher thermal gap working temperatures, therefore the contribution of alternative energies is reduced and investments in these systems are not amortizable. Compared to forced or convective air systems, where HFC refrigerants or water coolants are used at high and low temperatures, the energy performance is much greater [46]. Today's solar energy and geothermal energy technologies and performance are ideal to use with the system and will be even more appropriate with the arrival of technological advances in the near future.

4.1. Solar Energy Contributions to the System

Low-temperature solar thermal energy is perfectly adapted to circulating the water temperature requirements of a radiant surface heating system. Flat plate solar panels or solar thermal collectors heat the water, depending on latitude and sun, at temperatures below 90 °C for its subsequent distribution into the closed circuits. The system requires the setup of another supporting source of energy for those moments in which the water's thermal gap does not guarantee sufficient power to counteract the served spaces' thermal loads. The lower the solar collector's working temperature, the greater its performance. For average temperatures of water circulation as a heat transfer fluid between 35 °C and 45 °C, performance values of around 40% are common in winter for climates such as that of the Spanish Mediterranean [47].

In the winter regime, the heating behaviour improves when it is underfloor. The air temperature gradient surrounding the individual is closest to the ideal human comfort curve (ASHRAE). The surface temperature of the floor should not exceed 29 °C, as it can cause blood circulation problems. The temperature can be higher in roofs or walls and achieve a greater emission power.

In the case of capillary tube systems, either underfloor or in the ceiling, the usual cement mortar layer of thick tube systems may not be installed, meaning that the system would lack thermal inertia. In this case, hot water storage tanks should be used from which, by means of a secondary circuit, the hot water would be distributed to substation exchangers at the appropriate temperature of 45–35 °C. A heat pump, boiler support, or auxiliary system would solve the energy demands when thermal gaps are insufficient. In the Spanish Levante, and specifically in Alicante, a sunny winter day does not usually offer more than 5 h of sufficient solar power [48]. During the remaining solar hours, the system

is able to contribute between 30% and 60% of the heating, completed by a heat pump or a natural gas boiler. In summer, the solar useful hours exceed an average of 9 h a day, and cloudy days are few. The system is thus capable of contributing between 60% and 80% of the space cooling energy consumption, which usually allows the investment to be amortized in about 10 years [49].

Figure 5 shows the circuit diagram with the contributions of solar energy as a support system. The water in the solar thermal panels primary circuit heats the tank water up to 60–80 °C. Depending on the tank's size, it is possible to obtain greater inertia in the system to solve nighttime demand. From this point, a primary circuit is distributed to the substation exchangers, and different PPR capillary tube circuits are distributed from there. In segments with sufficient thermal gaps, the energy consumption would simply total that of the two water circulators.
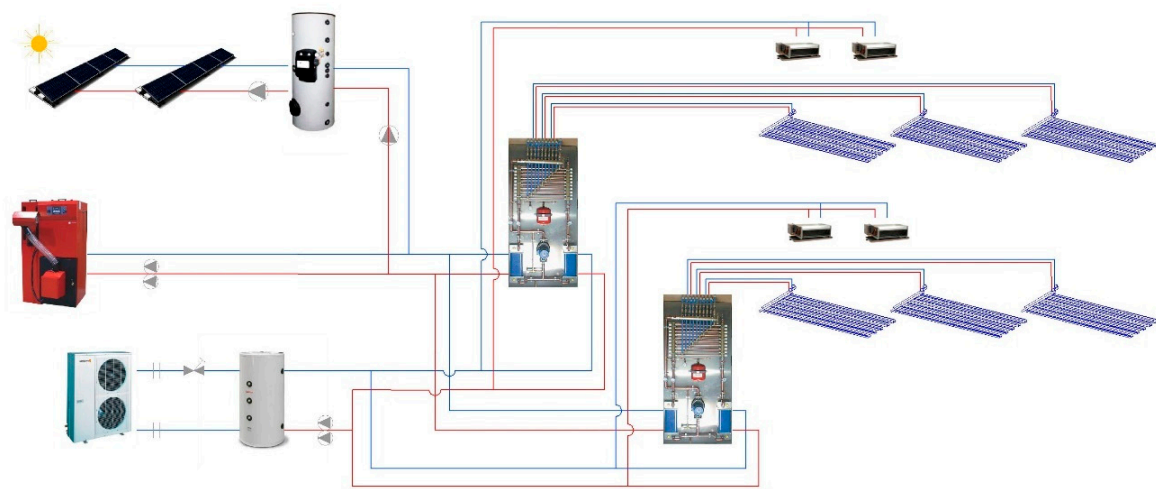
Figure 5. The circuit installation diagram based on three tubes with substations.

4.2. Solar Energy: Absorption and Adsorption Systems

So-called "solar cooling" systems are based on the use of solar radiant energy to cool water in a closed circuit to support adequate air conditioning. It basically consists of transforming solar energy for air-conditioning in summer, obtaining sanitary hot water throughout the year, and reinforcing heating in winter. This system guarantees savings of up to 70% since, on the one hand, a renewable energy source is used, and on the other, electricity consumption is reduced. With these systems, the environmental impact is minimized, reducing gas emissions (CO_2, SO_2, and NO_x) as well as non-renewable raw materials, such as fossil fuels.

Solar cooling systems present a major advantage of being used when the maximum levels of demand and production coincide since a building's air conditioning needs increases when most solar radiation is produced. The systems are especially efficient and suitable for buildings requiring intensive cooling and heating, as in the case of ever more comfort demanding residential and tertiary sectors (hotels, shopping centres, offices, single-family homes, etc.). To avoid solar panel overheating problems in summer, heat dissipation systems that produce the required energy dispersion exist. Usual solutions include cooling towers, pools in the case of houses, cooling wind turbines, etc.

For these types of facilities, it is necessary to dispose of a heat pump or boiler and a cooler to support the solar cooling production system and to provide for cases where solar produced hot water is insufficient. Two technologies have been developed for solar production: absorption and adsorption. The former, in turn, is divided into absorption systems with lithium bromide, and triple phase systems without refrigerant, using lithium chloride.

4.2.1. Refrigeration by Absorption

An absorption machine is a device that transfers energy from a low-temperature source to a high-temperature source, with a little added energy consumption. It consists of a heat pump, but, unlike mechanical compression systems in which energy is transferred by changing the state of some substances when passing from gas to liquid and vice versa, it works thanks to the capacity of certain substances to absorb a cooling fluid. In this sense, the compression is thermal instead of mechanical. Unlike electric heat pumps, the energy provided is thermal, which is why they are suitable for being coupled with solar collectors or other heat sources [50]: biomass boilers, natural gas boilers, cogeneration, heat recovery systems, etc. Depending on the refrigerant and absorbent fluid, the absorption machines can be divided into:

- Lithium bromide: water (refrigerant) and lithium bromide (absorbent).
- Ammonia: ammonia (refrigerant) and water (absorbent).

These machines produce a thermal gap of approximately 5 °C between the supply and return of the water distribution circuit to the exchangers of the capillary tube substations and the fan-coils responsible for dehumidification. In the case of lithium bromide systems, the flow temperature is around 10 °C and 15 °C on return. These systems present major energy and environmental advantages. They reduce CO_2 emissions in the atmosphere proportionately to electrical energy savings and they can rely on renewable energy [51].

4.2.2. Refrigeration by Absorption. Chemical Energy

Triple phase absorption technology stores and integrates solar energy in a different way from that described above, enabling the stocking of chemical energy. The process alternates between cycles of three aggregation states—solid, liquid, and gaseous—enabling continuous cooling or heating power. The devices can operate in three different modes: charging, heating, and cooling. The charging mode stores energy by drying a salt (Lithium Chloride—LiCl) that can be used later when necessary. Noteworthy is the fact that the machine can load and unload simultaneously. This means that it can receive thermal energy on a constant basis and, at the same time, supply heat or cold (heating and cooling). The system can also simultaneously heat domestic hot water (DHW) or a pool [52].

These modular absorption machines have been designed to use relatively low temperatures, so they are optimized for use with solar thermal collectors. They also work with stable temperatures inside the accumulators, which allow for the efficient use of solar thermal collectors. Devices designed to solve air conditioning in single-family homes, based on two parallel barrels, with a maximum cooling capacity of 20 kW, a heating capacity of 25 kW, and only 30 kW of input power exist.

In the refrigeration process, the higher the temperature towards the distribution system, the greater the efficiency. It is thus ideal for radiant floor, ceiling, or wall applications in which temperatures around 17 °C are used, such as PPR capillary tubes. The thermal COP is approximately 0.68. To illustrate how it operates, if the heat sink temperature was 30 °C, and we supplied 15 °C to the capillary tube cooling circuit, the power of each barrel would be 9 kW, i.e., a total of 18 kW. When 70% of the energy is discharged, the cooling power will be 14 kW, i.e., 4 units lower.

In the heating process, an opposite cooling phenomenon takes place. The charged energy is extracted in the form of heat. The water returns from the capillary tube distribution system to a temperature lower than that of the reactor's. It is thus ideal for radiant floor, ceiling, or wall applications, with temperatures around 27 °C. The thermal COP is approximately 0.85. A source of support heat should be used for very cold days, or when the thermal gap in the solar collectors is insufficient. If the heat sink temperature provides 10 °C and 30 °C is supplied to the heating circuit by radiation, the heating power would be 7.5 kW.

These systems need the excess energy to be dissipated efficiently and in a technically feasible way. In the case of single-family homes, this can be easily solved by using pool water, the foundations, or the land, but in the case of collective housing buildings, the solution becomes much more complicated.

Figure 6 shows a circuit diagram of this installation, with cold water distribution circuits to the capillary tubes and fan-coils. It is noteworthy that among other applications, capillary tube mats are ideal to ensure energy surplus transfers with swimming pools, building foundations, or land.
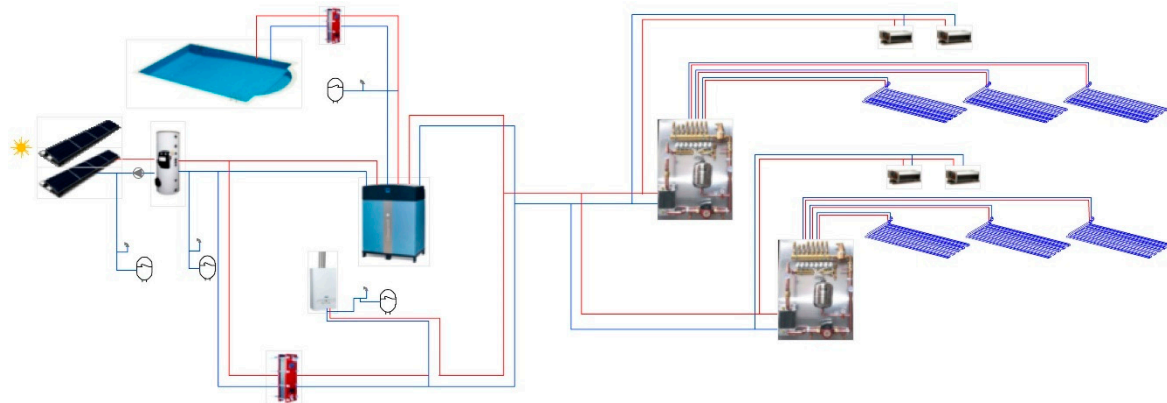
Figure 6. The circuit diagram with the accumulation of chemical energy based on lithium chloride.

This system entails significant energy savings compared to conventional compressor heat pumps since the absence of a compressor means it hardly requires any electricity consumption. Given that most electrical energy is produced by the burning of fossil fuels with their resulting CO_2 emissions, these emissions are significantly reduced. A typical Spanish household could save around 15 tons of CO_2 a year by using this system. It would seem sensible that competent authorities pay attention to these new technologies and favour their implementation by offering subsidies proportionate to the emission quota benefits obtained.

4.2.3. Refrigeration by Adsorption

Unlike absorption machines, in adsorption devices, a solid adsorbent is used instead of a liquid absorber. The operation cycle is not continuous and there is a loading phase as well as a discharge phase. The COP is between 0.55–0.65 and the hot source temperature can be lower than that of the absorption machines (from 55 °C), which uses flat solar collectors. The adsorption machine uses water as a refrigerant and silica-gel as an adsorbent. They are made up of four components: 1 evaporator, 2 adsorbent chambers, and 1 condenser. In the evaporator, water at low pressure evaporates, cooling water from 11.7 °C to 6.7 °C, or at the required temperatures and it is able to cool water up to 6 °C to 3 °C [53]. Water evaporation is adsorbed in one of the adsorption chambers by the dehydrating agent (silica gel), which becomes saturated. By means of a cooling tower, the devices' cooling water is cooled down to the necessary temperature to be able to be introduced back into the equipment.

5. Case study. Description of the Home and Its Northeast Enclosure

The building under study was located in the urban area of Alicante city (Figure 3). This corner building has a façade giving onto Benito Pérez Galdós Avenue and another giving onto Catedrático Ferre Vidiella Street. The building houses 69 flats with 2, 3, or 4 bedrooms; garages; and storage rooms. It has 9 different types of homes (flats A–F, penthouse types N–P). It has a corner building between the party walls, with a ground floor, 6 more floors, and a loft. There are 5 vertical communication nuclei.

The home under study was one of the building's type C flats (Figure 7). It consisted of 2 bathrooms, 4 bedrooms (2 bedrooms giving onto the interior patio of the building measuring 4×4 m^2 and 2 bedrooms giving onto the block's interior courtyard), a living room, and kitchen oriented towards the façade giving onto Benito Pérez Galdós Avenue (Figures 8 and 9). None of the flat's boundaries corresponded to the party wall.
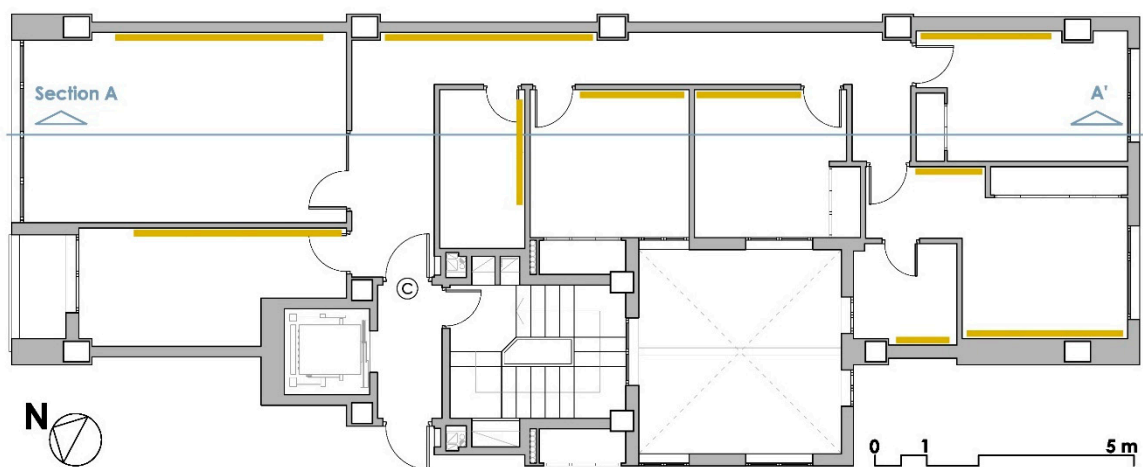
Figure 7. The northeast view of the building.

Figure 8. The general floor view of a type C flat. Thermal ceramic panels (TCP) in yellow.
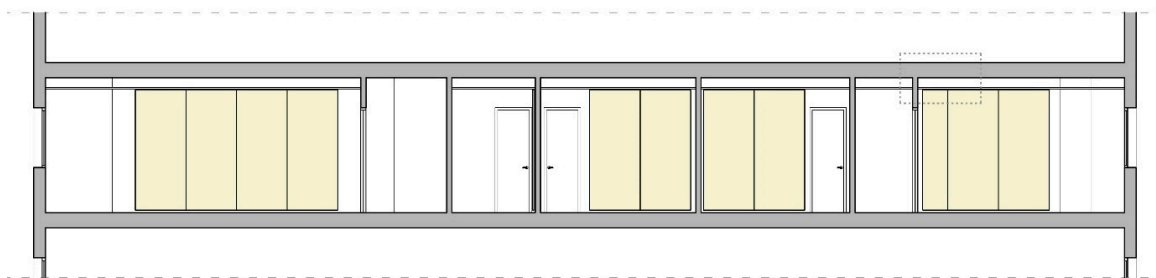

Figure 9. The cross-section of the home under study. Thermal ceramic panels (TCP) in yellow.

6. Monitoring of the Northeast and Southeast Façades

The monitoring equipment was installed after the construction of the building. To install some of the surface temperature sensors, a quasi-circular surface of around 40 cm in diameter had to be destroyed since four layers of the façade had to be broken The apparatus installed included sensors for measuring relative humidity of the outdoor and indoor air, the surface temperature in the different parts of the enclosure, solar radiation using a pyranometer located 1 m away on the façade, indoor air velocity, external cavity air velocity, and temperature (Table 2). Temperature sensors (PT 100) were placed in each of the layers of the façade's enclosure (Figure 10 and Tables 3 and 4). Due to the risk of interstitial condensation, a humidity sensor was placed in the layers of the enclosure [35].

Table 2. The general map of the sensor system to monitor the type C flat.

Field Devices (Indoor and/or Outdoor)	Building (Alicante)
Temperature-humidity sensor for outdoor environment	1
Temperature-humidity sensor for indoor environment	1
Interstitial temperature-humidity sensor	2
Solar radiation sensor	2
Air velocity sensor	1
Temperature sensor	23
TOTAL	30

Table 3. The description of the sensors and measurement units.

Key	Measure	Unit
N1	Temperature	°C
N2	Temperature and humidity	°C, %
N3	Temperature	°C
N4	Temperature	°C
N5	Temperature	°C
TE-HE	Outdoor temperature and humidity	°C, %
Ti-Hi	Indoor temperature and humidity	°C, %
An	Airspeed	m/s

Table 4. The description of the building materials that make up the enclosure and the floor slab.

No.	Materials	Thickness (cm)
1	Gypsum plaster	1.0
2	Hollow ceramic brick	11.5
3	Perforated ceramic brick	11.5
4	Polyutherane foam	3.0
5	Structural support. Metallic structure	10.0
6	Ventilated air chamber	7.0
7	Porcelain stoneware	1.0
8	Marble paving	2.0
9	Grip mortar	2.0
10	Base mortar layer	4.0
11	Anti-impact coating	0.3
12	Reinforced concrete slabs	30.0
13	Plaster coat	1.5
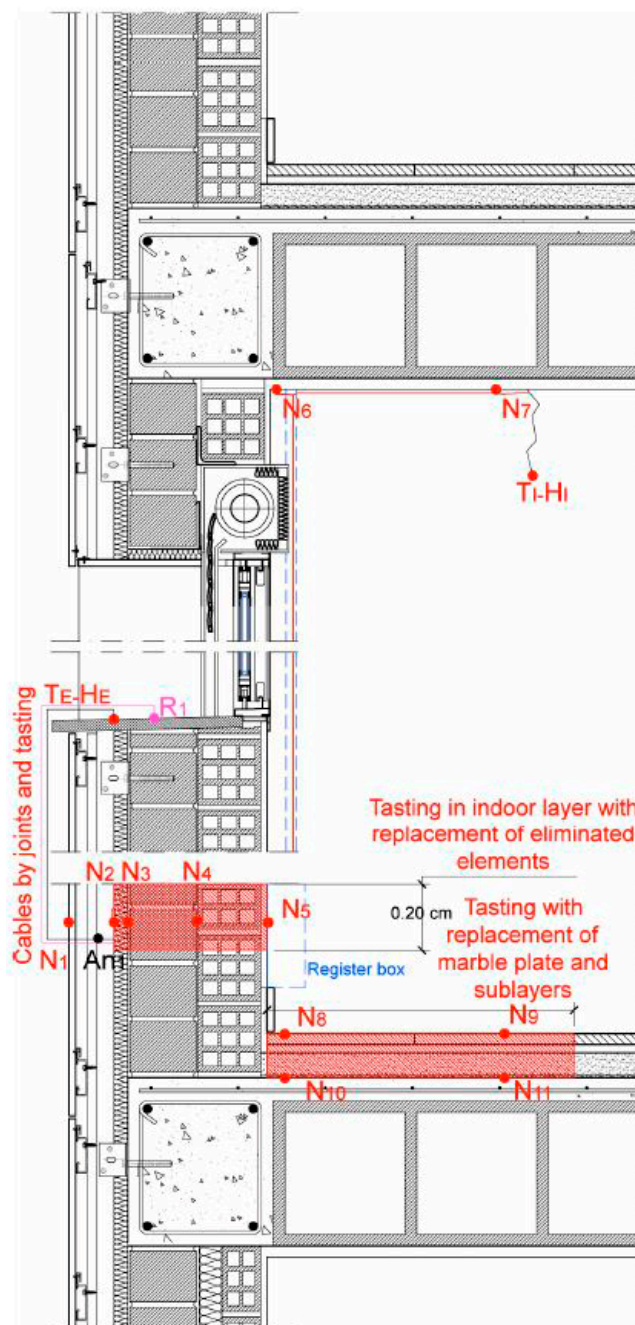
Figure 10. The sensor location chart.

6.1. Description of the System Connection Flow Chart

The monitoring system consisted of the sensors, placed at strategic points in the building's two façades, determined according to the physical composition of the glazing and front slabs. Data collected by the sensors were sent to a data logger (analyser), which transmitted the signal via general packet radio service (GPRS) to a database. This information was accessible from a web platform.

6.1.1. Description of the Analyser

The global system for mobile (GSM/GPRS) data logger GRD (gradual decoding refresh) recorded data via analogue or digital channels. Through its GSM/GPRS modem, the data were sent to a server and could be consulted on the web in graph or table formats (Figure 6). They could be downloaded as CSV files as well.

6.1.2. Description of the Sensors

The technical characteristics of the data logger and sensors are as described below.

6.2. Data Reception System

The GPRS GRD data could be viewed on the web in graph or table formats and downloaded as a CSV file as mentioned above. The web interface provided a control panel to configure a personalized view, showing the data of all the sensors remotely. Data were collected for the complete 2014 and 2015 yearly cycles, based on data captured every half hour every day, although it was mainly the 2015 data that were analysed.

Time ago, the sensors were introduced after the completion of the building. The sensors were introduced to the surfaces according to the location layout shown in Figure 10. The damage to the enclosure was repaired once the sensors were placed with connecting cables to the analyser (Figures 11 and 12). The various layers of plaster, hollow brick, perforated brick, polyurethane, etc., were sealed back to ensure maximum continuity with the original materials. (Figure 12).


Figure 11. The location of sensors N_1 to N_5 in the enclosure layers.
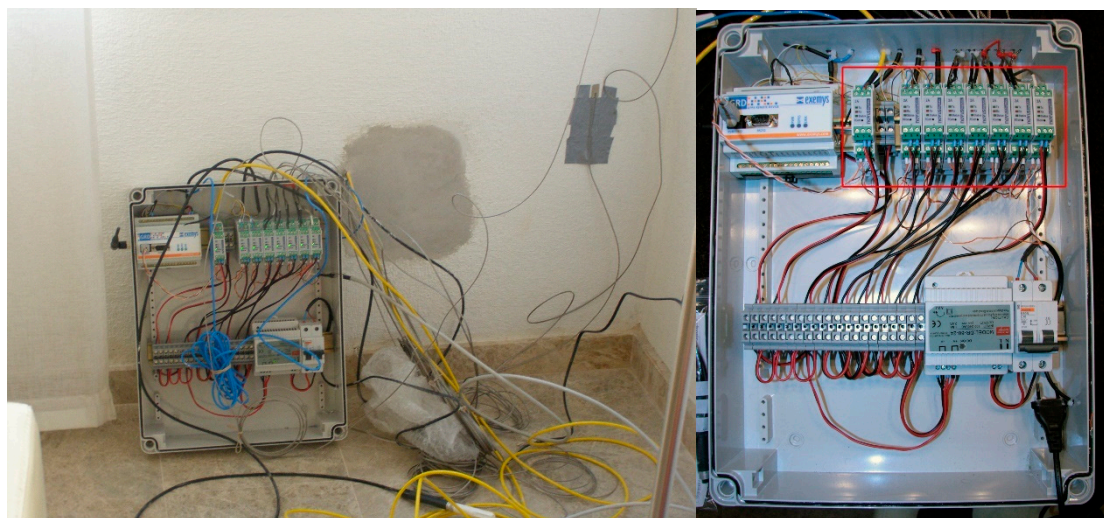
Figure 12. The data logger, data reception, and general packet radio service (GPRS) communication.

A thermal flow measurement of the opaque enclosure was carried out, to obtain the U-value [54,55] in accordance with ISO 9869-1: 2014 [56]. Data were analysed using the module for calculating thermal transmittance included in the AMR WinControl software developed by Ahlborn for the ALMEMO measuring equipment. The "average method" [57] was used. The results are shown in Figure 13 and Table 5.
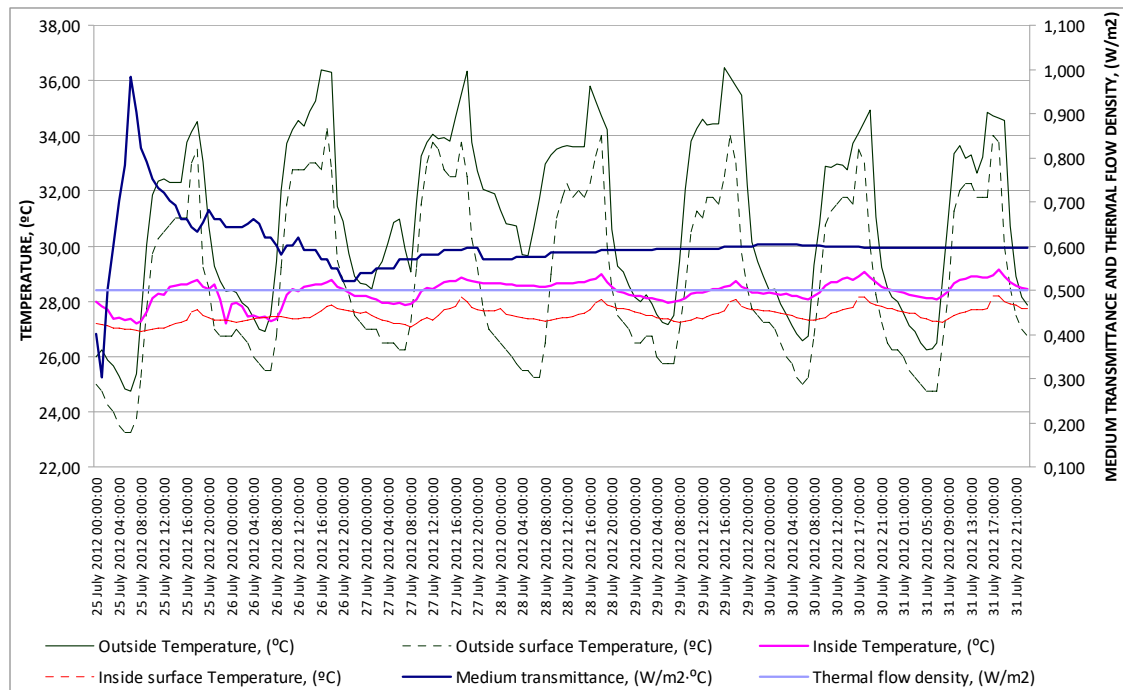

Figure 13. The thermal flow measurement graph with the temperature and flow data used to calculate the *U*-value.

Table 5. The *U*-values obtained in the different scenarios.

	Fourier UNE	**Fourier Mathis TCi**	**Monitoring C$_1$**	**Monitoring C$_2$**
U (W/m^2°C)	0.437	0.497	0.526	0.545

The heat flow analysis was completed by thermal imaging and the detection of thermal bridges (Figure 14), which helped to determine the behaviour of the outer envelope in the air chamber [58,59]. Then, the thermal bridges were quantified to perform thermal behaviour simulations [60].
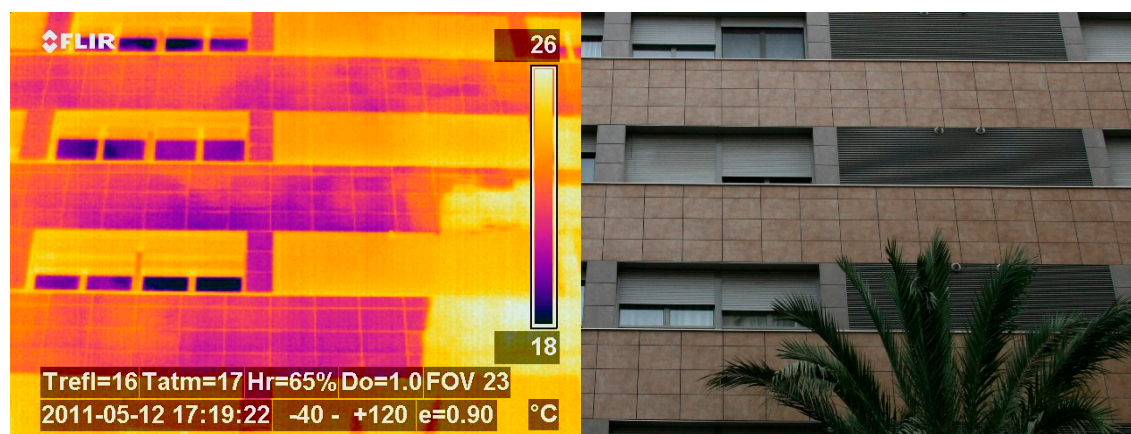
Figure 14. The thermographic image of the northwest facade. Taken on 12 May 2013, at 3:55 p.m.

The results obtained by monitoring were corrected by a specially designed algorithm [35]. They were used to calibrate the design builder tool and validate the building's thermal behaviour simulations. They also analyzed the effect of thermal inertia on the enclosures, together with the produced thermal waves and their effects on surface temperatures and indoor air temperature, enabling the adjustment of indoor comfort conditions (Figure 15).
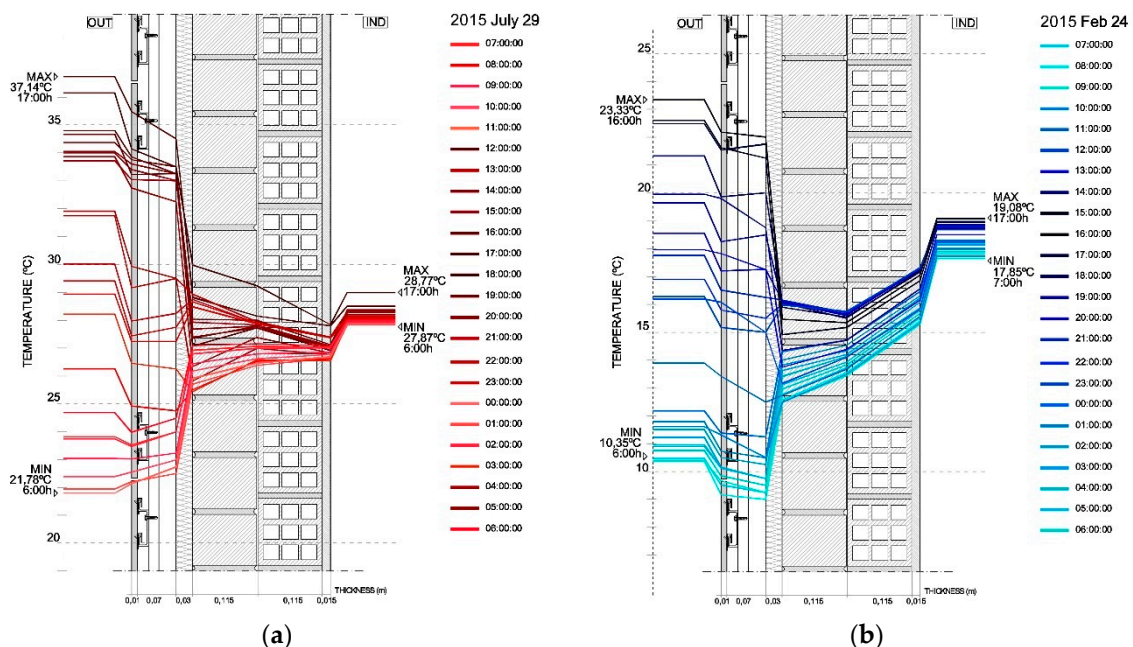

(a)   (b)

Figure 15. The temperate gradients for each hour. (**a**) 29 July 2015; (**b**) 24 February 2013.

7. Calculation of Conditions of Comfort

The objective of this research was to compare two well-differentiated systems of air conditioning, mainly through the energy consumption and savings that would be derived from the use of TCP panels combined with thermal solar panels on the roof, to cool or heat the air conditioning system's water [61]. For this, calculations of the optimal surface for the home's air conditioning were carried out. A total of 72.5 m^2 of TCP panels and 18.5 m^2 of solar thermal panels were required. The thermal performance ratios of 1 m^2 of solar thermal panels in similar climates were taken into account for the dimensioning [62]. There were 329 days of sun in Alicante in 2015. The energy captured in summer was 819.75 kWh/m^2/year and 438.91 kWh/m^2/year in winter, leading to an annual total of 1258.66 kWh/m^2/year. Panel performance was estimated at 84.5% according to the usual ratios [63]. The necessary power for good energy contribution to the system was taken into account.

This comparison, however, could only be accomplished by setting the parameters that guaranteed similar user comfort in all the scenarios under analysis. In previous studies, comparative results of the user's energy losses were obtained [30], setting the operating temperature value T_o according to the values established by the RITE, the Spanish regulations included in the CTE [11]. A T_o of 21 °C was set for winter and 24 °C for summer. In order to evaluate comfort, the user's energy loss values were obtained from Equations (1) to (7) (Section 2). The results are shown in Table 6. As can be observed, the indoor air temperature in the case of the TCP panel KaRo capillary system was about 2.1 °C higher in summer and 1.5 °C lower in winter, with similar levels of comfort to that of the VRV split convective system. The individual's energy losses underwent a slight variation, mainly due to the fact that the air velocity in the occupation zone was 0.05 m/s in the TCP system and 0.15 to 0.18 m/s in the VRV split system, but the T_o operating temperature remained constant. Given that the usual comfort values of individual losses are around 85–95 W at rest, and 100–120 W during moderate activity, we can conclude that the house provides good comfort levels, though they could be insufficient during peaks loads.

Table 6. The individual heat transfer in the summer regime in the living room.

		v m/s	h_c W/°C	T_p °C	T_a °C	h_r W/m²°C	T_{rm} °C	q_{cvi} W	q_{rdi} W	Total W
Summer	OP 1	0.160	9.081	30.00	23.37	4.70	24.70	60.20	24.91	85.11
	OP 2	0.050	6.875	30.00	25.48	4.70	20.18	31.08	51.54	82.53
Winter	OP 1	0.192	9.495	30.00	23.11	4.70	21.45	65.42	40.18	105.60
	OP 2	0.070	7.450	30.00	21.61	4.70	23.75	53.56	29.38	82.94

Figures 16 and 17 show the data collected on relative temperatures and humidity, and on the indoor air temperature for a convective system and a climate control system with TCP panels, based on simulations in the Design Builder tool, during a week that was representative of summer conditions (1–7 August) and the winter regime (1–7 February).
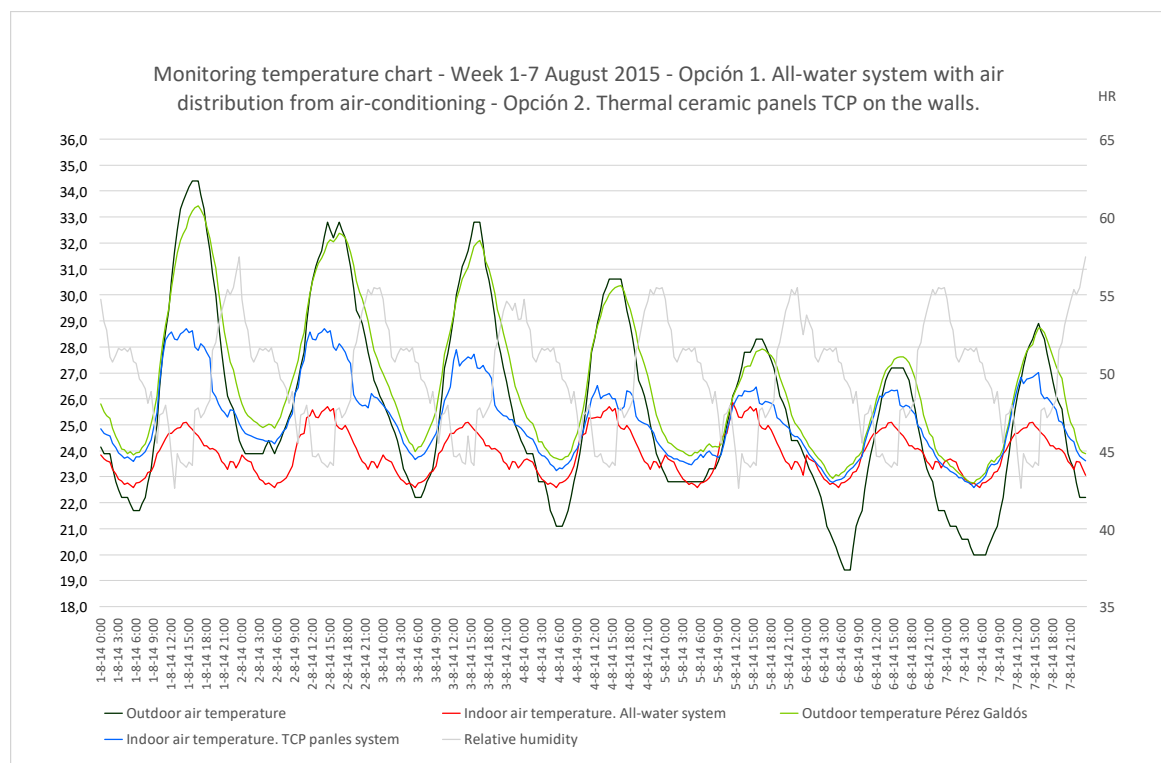
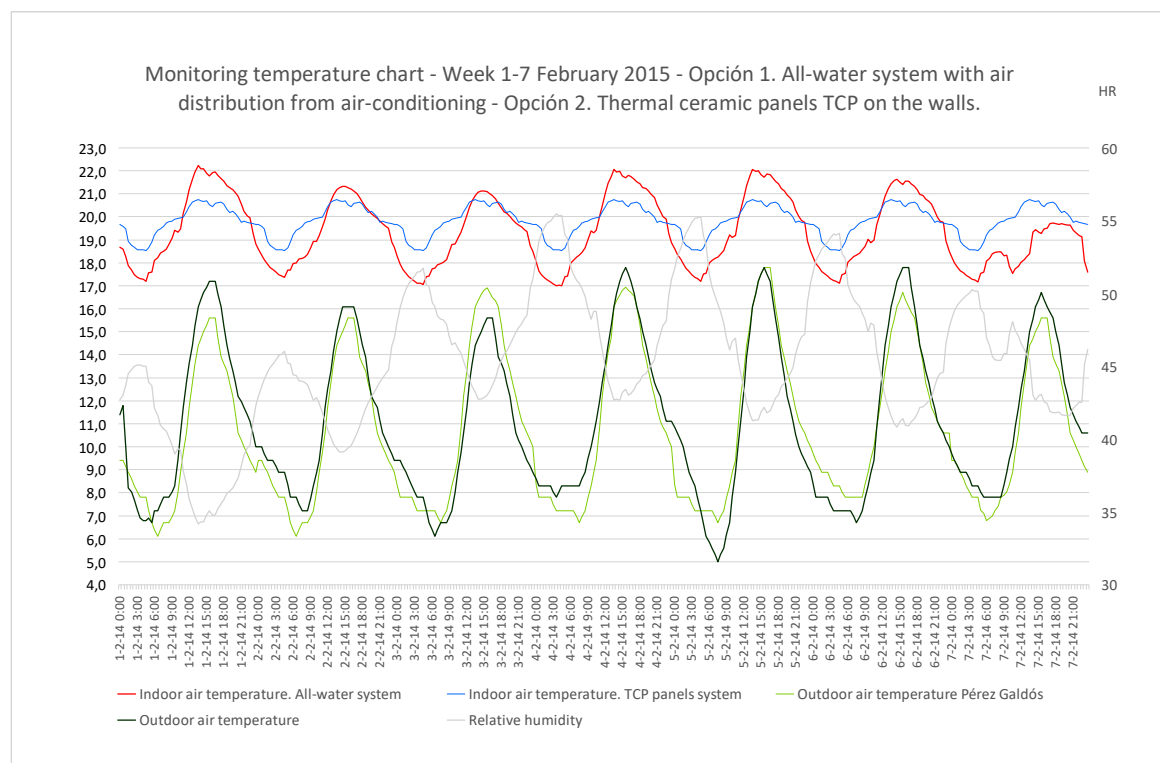**Figure 16.** The parameters of outdoor and indoor air during a summer week.

Figure 17. The parameters of outdoor and indoor air during a winter week.

## 8. Calculation of the Home's Energy Demand

The DB-HE technical document on energy saving [11], a mandatory regulation in Spain, envisages the application of the unified tool Lider-Calener (HULC) [12] to single-family and collective housing projects. The project model was created and a climatic data file, included in the tool and based on the population's location and altitude, was applied. The annual energy demand value was obtained, as well as its energy rating based on the air conditioning systems and energy sources used in the building. This tool is a big step forward, but it is still far from generating an adjusted or calibrated simulation reflecting the actual behaviour of buildings. It does not allow for the introduction of certain bioclimatic techniques [64] and some energies types prevail, motivated by insufficiently justified energy policies [4]. Finally, other tools such as Design Builder or TRNSYS make adjustments according to its actual use, such as window opening and closing time slots, or the use of enclosure thermal inertia for thermal comfort and energy demand reductions through phase change materials [13]. The Design Builder tool, which uses the modelling engine EnergyPlus (DOE), was used in this study (Figure 18).

To perform the building behaviour's simulations in terms of energy demand and indoor comfort parameters, the data described in this section was introduced into the tool. The winter period covered 1 December to 30 April, and the summer period 1 May to 30 November. The indoor air temperatures were wet to 21 °C in winter and 24 °C in summer. The occupation, for the standard calculation of air renewal, was set to 6 people. A value of 0.63 was set for the air changes per hour (acH) of air renewal, established in accordance with the current Technical Building Code (CTE). Air infiltration through the enclosure was moderate thanks to the quality of the frameworks and joinery. For evaluation purposes, the Blower Door test was carried out in accordance with the European Norm EN 13829 using the BlowerDoor GMBH MessSysteme für Luftdichtheit equipment (Figure 19). The results are shown in Table 7.
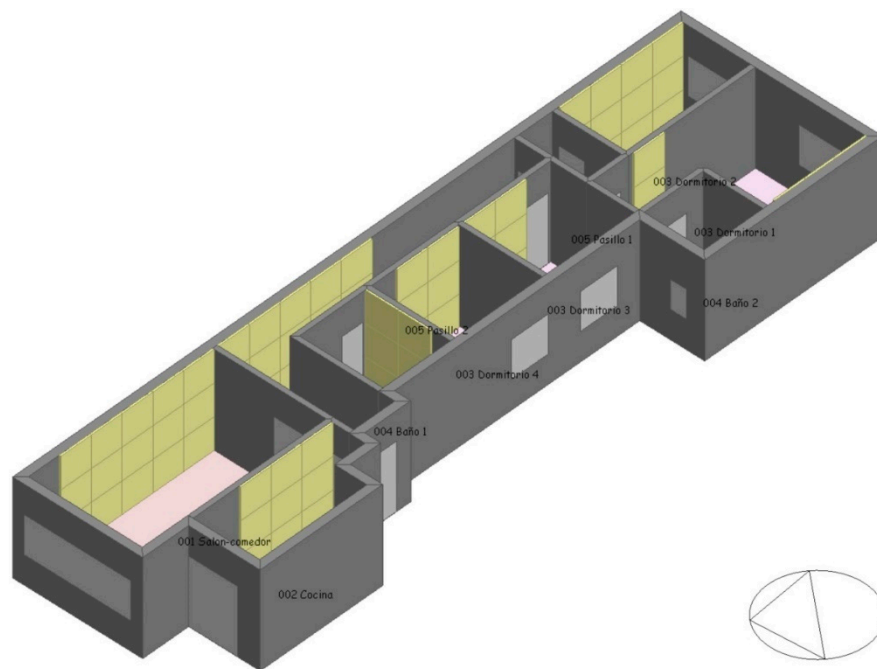
**Figure 18.** The model images in Design Builder. TCP panels are in yellow.
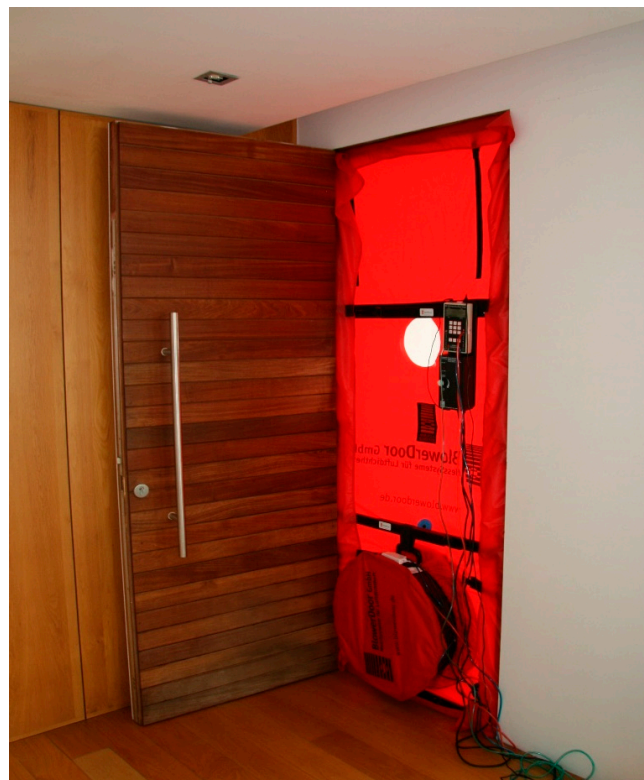
Figure 19. The blower door test. June 2015.

Table 7. The calculation of air infiltration in the envelope n_{50}.

	n_{50}	Total	Only Enclosure	n_{winter}	n_{summer}
Depressurization		3.10	2.81		
Pressurization		3.19	2.97		
Mean value	2.88 acH	3.15	2.88	0.314 acH	0.314 acH

To obtain the building's air infiltration average value—a parameter difficult to quantify—and to carry out simulations in Design Builder, the UNE-EN-ISO 13790: 2003 [65] standard was followed, and the value obtained in the test was applied to n_{50} (3.14 acH). The result was 0.342 acH, a low value for a single-family house in the Levante. We used the FLIR thermographic camera, the ThermaCam P 25, to detect thermal bridges (Figure 20). The quantification was carried out using the AnTherm program, estimating the gains or losses of load due to thermal bridges in 3.5% of total thermal loads [66] by enclosure U-values. Similar values were obtained in previous studies [67,68].
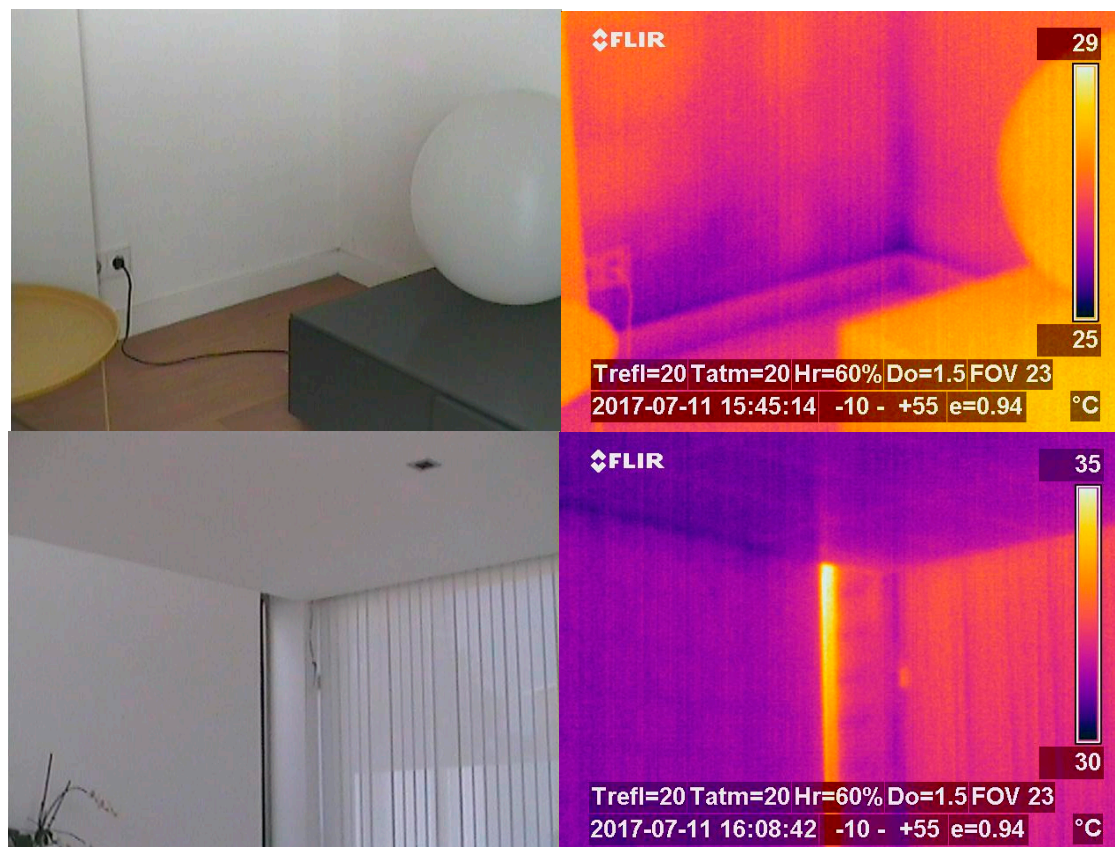
Figure 20. The thermographic images. Thermal bridges.

The project's circuit diagram of the capillary tube mats was introduced in the Design Builder model (Figure 21). To adjust the parameters obtained by simulation to the actual data, or to calibrate the model, the surface temperatures of the TCP panels were pre-set at 17 °C in order to avoid surface condensation risks. The climatic file relating to external air temperatures, relative humidity, and levels of solar radiation by pyranometer obtained in Alicante and reported in previous publications [31], was also introduced throughout the complete one-year cycle. The wall surface temperature was corrected and the infiltration value was adjusted to 0.342 acH. Thus the model was calibrated, adjusting the air and wall temperatures to the values obtained through monitoring. The dehumidification of the two fan coils was also applied, with a power of 1.85 kW and an energy consumption of 2350 kWh/year.
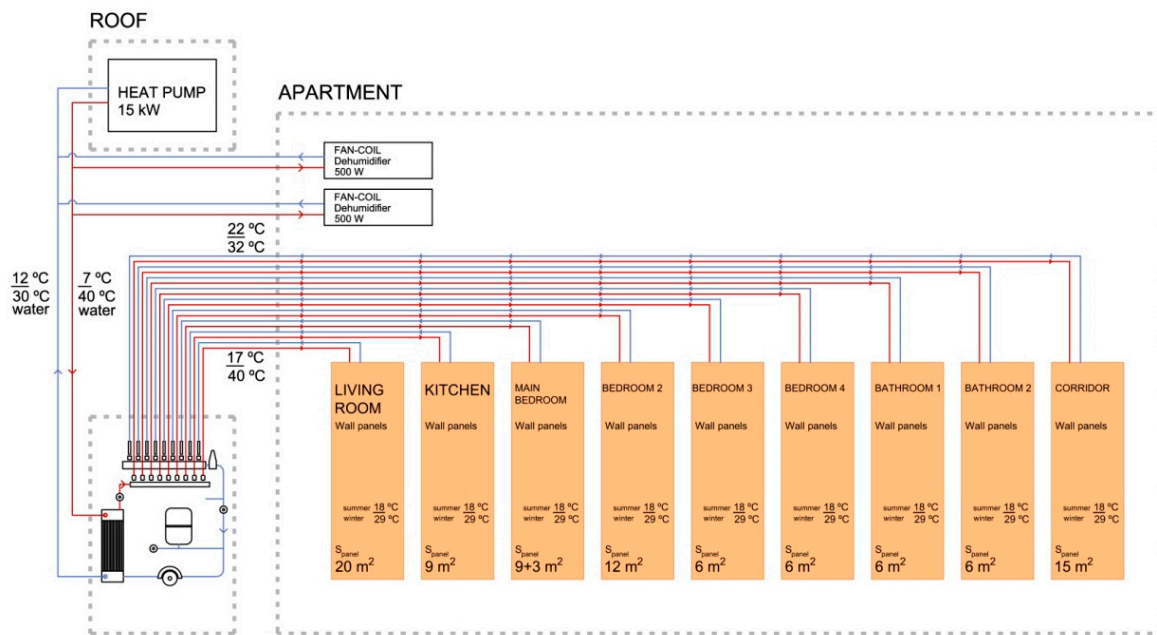
Figure 21. The circuit diagram of the installation of capillary mats and dehumidification by fan-coils. Modelled in Design Builder.

Once the above parameters of the CTE-based indoor air renewal rate, air infiltration, surface temperatures, occupation, etc., were obtained, the home's behaviour relating to the three options described above was simulated in order to analyse the user's comfort, the temperature gradients existing in the home's rooms, and to compare the summer and winter energy demands. As indicated, the indoor air setpoint temperature was 21 °C for winter and 24 °C for summer.

Summer, winter, and the annual energy demands, as well as the corresponding periods of amortization of investment, were compared for the three options treated in this study.

OP 1. All-air installation based on the VRV split system of reversible air-air heat pump, Performance™ 38MGR model by Carrier, 5 kW cooling capacity, and 5.47 kW calorific power. The conditioner was in in main bathroom, with cold or hot air ducts distributed throughout the house.

OP 2. Installation of PPR capillary tubes in TCP panels, with a Carrier model 30RH026 air-water heat pump, similar in power to OP 1; distribution of water to a substation located in a false wall in the corridor, and the distribution of water in the secondary circuit by 5 circuits of PPR with independent diameters of 20 mm to the whole house, and two fan-coils strategically located for the dehumidification of the air, with 1.2 kW of refrigerating power.

OP 3. Installation of capillary tube mats in PPR similar to OP 2, with the same heat pump as above, and the two fan-coils for air dehumidification, with a thermal solar panel system, absorption cooling, energy chemistry (solar cold), and providing alternative energy to the system (Figure 6).

These simulations produced the value of the energy demand in summer, winter, and annually for all three options (Table 8). The value was similar to that usually found for office building energy consumptions, for which savings have been demonstrated to reach between 30% and 35% compared to the convective systems in Central Europe [68]. In the case under study, the simulations produced annual energy saving values of 31.47% when using the TCP panels (OP 2) instead of convective systems VRV split (OP 1). These values are consistent with those found in other works [69]. Figures 22–25 show the temperature gradients produced by the simulation in the different areas of the house for the two air conditioning system options, OP 1 and OP 2. Drops and increases in air temperature were recorded at around 2.5 °C compared to the VRV split system air conditioning solution. To calculate the energy demand based on the setpoint temperatures referred to above, an all-air system was adopted, with air conditioning in the bathroom and the distribution of air by conducts to all the rooms in the house.
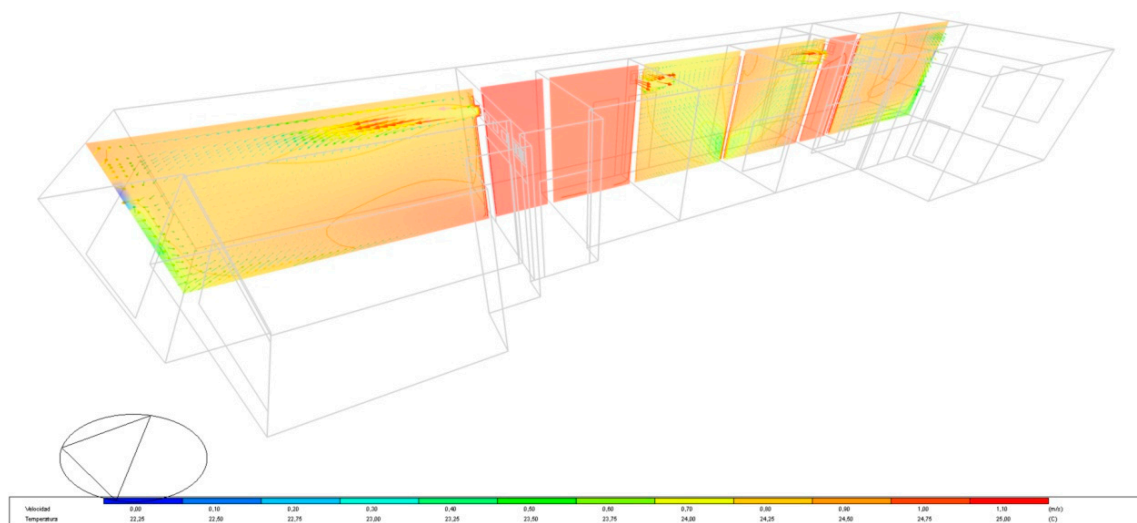
Figure 22. The all-air system with air conditioning and an air drive (convective); 1 August 2015, 4:00 p.m.
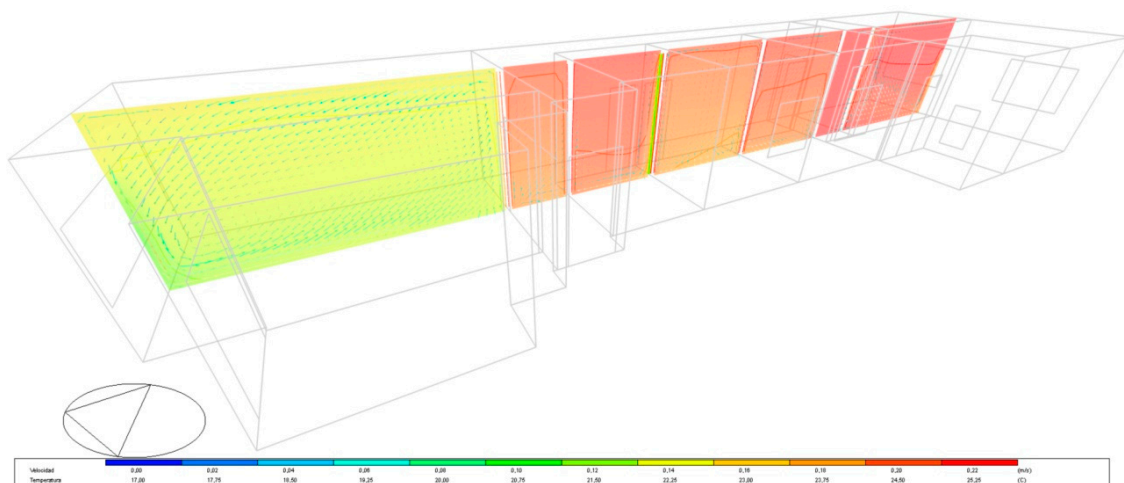
Figure 23. The radiant system using TCP panels; 1 August 2015, 4:00 p.m.
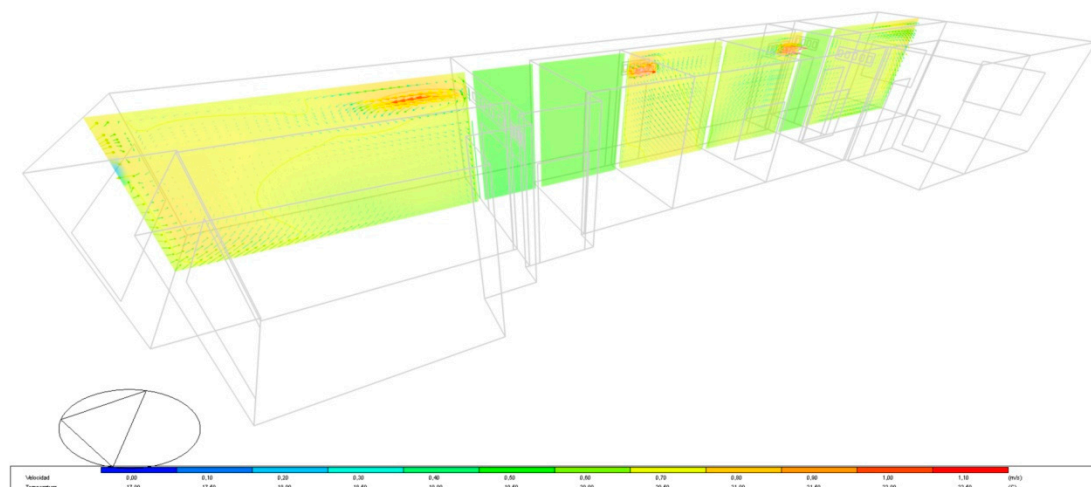
Figure 24. The all-air system with air conditioning and an air drive (convective); 1 February 2015, 9:00 a.m.
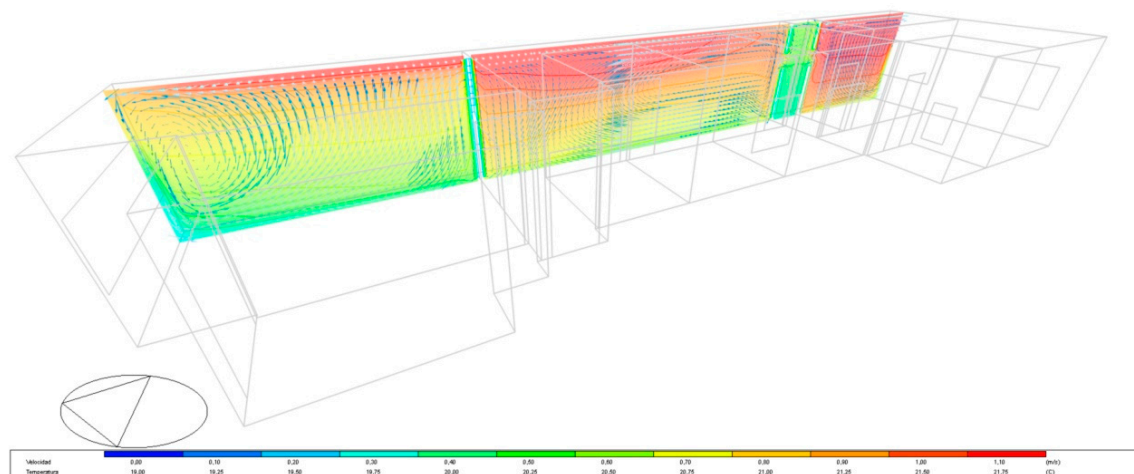
Figure 25. The radiant system via TCP panels; 1 February 2015, 9:00 a.m.

Table 8. The calculation of energy demands and CO_2 emissions of the 3 OP.

	OP 1	OP 2	OP 3
Summer Energy Demand, kWh/m^2	50.64	33.91	15.29
Winter Energy Demand, kWh/m^2	35.19	24.90	11.77
Annual Energy Demand, kWh/m^2	85.83	58.81	27.06
Annual CO_2 Emissions in Use Stage	3198.96 kg	2191.32 kg	1008.18 kg
Percentage	100.00%	68.52%	31.53%

To complement the simulations, the energy saved by using roof thermal solar panels [70], OP 3, heating the system water in winter, or cooling it in summer by an absorption cooling system or chemical energy (solar cold) was also examined [71]. Solar radiation power data for 2015 were collected using the pyranometer included in the monitoring installation. Figure 26 shows the values obtained for the representative months of August and February, and Table 9 presents the average daily values of energy captured each month and the total days of sunlight. These values were compared with other sources and publications, and correlative values were obtained [72,73]. The installation performance of 18.5 m^2 of solar thermal panels, with a latitude of 38° and an inclination of 45°, was 71.4% [74]. Given that the installation's overall performance was 84.5% [75], partly due to problems such as dust deposition in urban environments [76], the total contribution of energy to the TCP panel system was 4642 kWh/year.
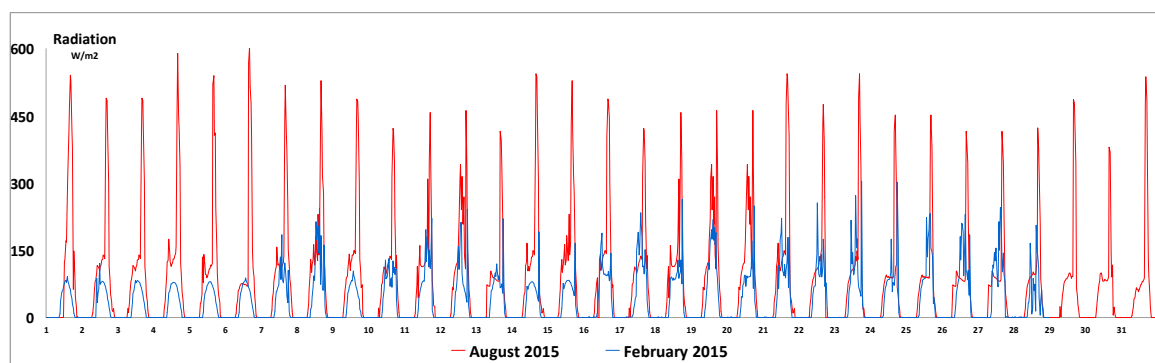

Figure 26. The solar radiation values collected in situ for the months of August and February 2015.

Table 9. The received solar energy per day, month, and year.

Month	No. of Days	Direct Irradiance (kWh/m² day)	Diffuse Irradiance (kWh/m² day)	Direct Energy per Month (kWh/m²)	Diffuse Energy per Month (kWh/m²)	Total Energy per Month (kWh/m²)
January	31	1.66	0.95	51.46	29.45	80.91
February	28	2.31	1.18	64.68	33.04	97.72
March	31	3.03	1.67	93.93	51.77	145.7
April	30	4.30	1.83	129	54.9	183.9
May	31	4.65	2.26	144.15	70.06	214.21
June	30	5.40	2.25	162	67.5	229.5
July	31	5.56	2.17	172.36	67.27	239.63
August	31	4.65	2.17	144.15	67.27	211.42
September	30	3.79	1.66	113.7	49.8	163.5
October	31	2.69	1.30	83.39	40.3	123.69
November	30	1.84	0.97	55.2	29.1	84.3
December	31	1.44	0.83	44.64	25.73	70.37
Annual radiation				1258.66	586.19	1844.85

The results obtained via the Design Builder simulation were calibrated and corrected based on these solar energy results and compared with other studies on thermal energy in similar climates [77]. The amount of energy saved by the system was 77.48% compared to all-air convective systems (Figure 27). These values are therefore significant and they reflect these systems' viability.
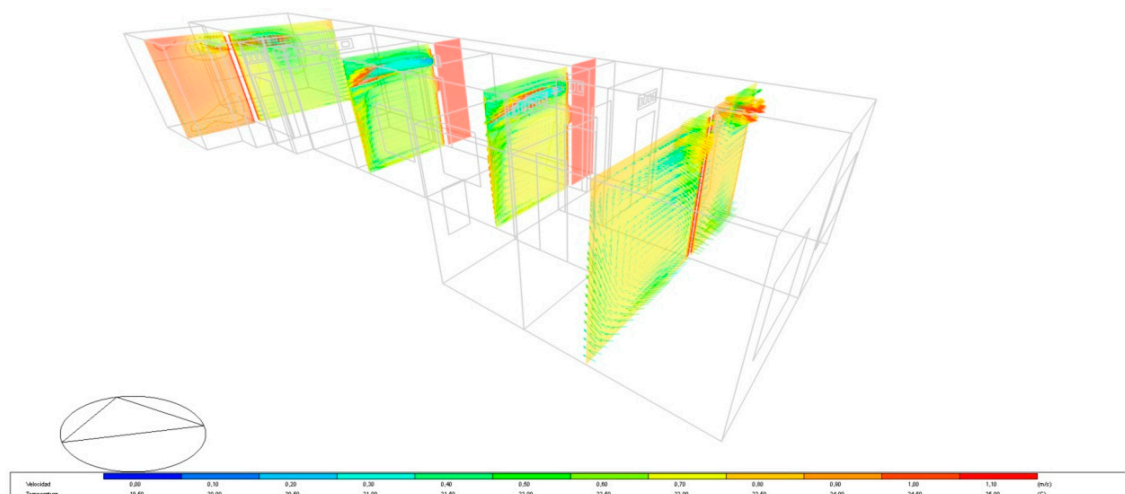
Figure 27. The all-air system in several sections; 1 February 2015, 4:00 p.m.

The energy consumption of the three analysed systems is detailed in Table 10 for all the equipment and elements of the analysed systems, as well as the solar panel energy contributions.

Table 10. The calculation of the annual energy consumption and comparison with convective systems.

	SUMMER from 1 May to 30 November WINTER from 1 December to 30 April Occupation: 4 PEOPLE	Unit	OP 1 All-Air System	OP 2 Walls TCP	OP 3 Walls TCP with Solar Panels
1	Effective Area	m^2	137.90	137.90	137.90
2	Ceramic panels area	m^2		72.5	72.5
3	Maximum thermal load	W/m^2	80	75	75
4	Minimum fresh air flow rate	m^3/m^2 h	1.70	1.70	1.70
5	Thermal jump of the water in summer	k	6	3	3
6	System running time	h/year	2160	2160	2160
	Ventilation				
7	Supply air flow rate	m^3/hm^2	16.52	2.31	2.31
8	Supply air volume	m^3/h	1.185	182	182
9	Fan power	kW	0.65	0.15	0.15
10	Power consumption	MWh/year	2.31	0.51	0.51
	Cooling pump				
11	Water flow rate	l/m^2 h	10.70	21.5	21.5
12	Volume of water	l/h	1475	2965	2965
13	Power	kW	0.10	0.25	0.25
14	Power consumption	MWh/year	0.22	0.43	0.43
	Fans and pumps				
15	Power consumption	MWh/year	2.53	0.94	0.94
16	Comparison	%	100%	37.3%	37.3%
	Fan-Coils Dehumidifiers				
17	Power	kW		1.85	1.85
18	Power Consumption	MWh/year		2.35	2.35
	Cooling system				
19	Emission power	W/m^2	85	69	69
20	Power	kW	8.87	6.34	6.34
21	Summer power consumption	MWh/year	3.83	2.09	2.09
	Heating system				
22	Power	kW	8.07	6.75	6.75
23	Winter power consumption	MWh/year	2.90	1.81	1.81
24	Solar energy supply	MWh/year			–4.642
	Circulators of water to the system				
25	Power	kW			0.12
26	Power consumption	MWh/year			0.26
27	Annual power consumption	MWh/year	11.848	8.116	3.734
	Comparison	%	100%	68.53%	22.52%

As can be observed, the split VRV system energy consumption for air distribution was 267% higher in OP1 than the water distribution in OP 2 and 3. The energy consumption in OP 2 was 31.47% lower for the reasons described in Section 3. Consumption due to dehumidification, with the two fan-coils of OP 2 and 3, represented 2.35 MWh/year, i.e., 25% of the total OP 1 consumption, making the TCP panel installation apparently less favourable. However, the savings from the transported water energy compared to that of air, as well as the thermal load reductions due to the thermal gap drop in the enclosure transmissions, mean that the system as a whole generates notable energy savings compared to OP 1.

CO_2 emissions in the electric mix were quantified using the ELCD database [78,79], according to which, to produce 1 kWh of electricity, 0.41 kg of CO_2, 0.00122 kg of CH_4, and 0.0000465 kg of N_2O are released. The final user energy consumption was then quantified. To finish, the primary energy consumption and CO_2 emissions were obtained based on the IDAE factors for 2010, specifically 2.21 MWhp/MWhf and 0.27 tCO_2eq/MWh.

To complete the comparative analysis, we estimated the profitability of the potential technical investments in the Spanish Levante collective housing. To calculate the installation costs, databases of the companies in the sector were used [80]. The cost of 18.5 m^2 of solar thermal panels was calculated based on a ratio of 261 €/m^2, which includes the cost of labour, storage tanks, distribution equipment, circulation pumps, equipment system management, and annual maintenance costs. The total estimated

cost amounted to €9037. The cost of the investment in the installation system of 72.5 m^2 of KaRo mats, including the substation and 20-mm diameter PPR tube circuits was 58% higher, therefore, the investment's amortization period could be calculated as shown in Table 11. To calculate the amortization periods, a cost of 0.132 €/kWh was applied [51]. As can be observed, the investments were amortized over the long term, between 15 and 23 years. To make decisions about the possible implementation of these systems, we must bear in mind the high comfort standards provided to homes, as well as the significant CO_2 emission reductions due to a 31.47% (OP 2) and 77.48% (OP 3) drop in the annual energy demand. This is a determining factor in the life cycle assessment (LCA) of the system. [81]. These CO_2 emission reductions could be encouraged by public administrations, thus, reducing the users' installation costs, leading to shorter amortization periods.

Table 11. The calculation of the investment amortization period of OP 3 compared to OP 2.

Investments and Pay-Back Periods	Unit	OP 1	OP 2	OP 3
All-air installation with heat pump	€	19,820		
Capillary tubing weft with TCP panels	€		31,317	40,354
Annual energy consumption	kWh/year	11,848	8116	3734
Annual savings	€		493	578
Amortization period	years		23.31	15.67

9. Conclusions

Radiant surface conditioning systems using PPR capillary tubes are very efficient, they achieve high comfort standards and significant energy savings, they are healthier and more environmentally friendly. Taking the case of the Mediterranean coast, it was possible to experiment and evaluate their performance in an apartment block flat located in Alicante. Three scenarios were examined. The first scenario consisted of using an air conditioning system based on a VRV split convection system (OP 1). In the second scenario, an air conditioning system by radiant surfaces was used, based on TCP thermal ceramic panels on the wall, incorporating PPR capillary tube frames (OP 2). The third scenario was a variant of the previous one: thermal solar panels on the roof were incorporated by providing renewable energy to the system (OP 3).

- The TCP panel systems were more efficient in terms of energy and more comfortable than OP 1. The annual energy demand was 31.48% lower in OP 2 and 69.47% lower in OP 3.
- User comfort, based on the T_o operating temperature and the ability to transfer energy to the environment, was 27.3% higher in OP 2 and OP 3 in the living room, and 19.7% higher in bedroom 1. In this scenario, although the indoor air temperature was around 2.1 °C higher in summer and 1.5 °C in winter, because the value of the average temperature radiant T_{rm} for summer was 4.52 °C and 2.31 °C lower for winter, the resulting operating temperature T_o improved compared to the convective conditioning systems (OP 1).
- Investments in installing the capillary tube mat system using TCP panels could be amortized within a reasonable period of time compared to a convective VRV split system based on a heat pump, an evaporator in the bathroom, and distribution by ducts (OP 1). For the home under study, the extra cost of €11,497 could be amortized in 23.31 years, with a 3732 kWh/year drop in the energy demand and a €493 saving per year, with a cost of 0.123 €/kWh in the electric mix.
- If 18.5 m^2 of solar thermal panels were also installed on the roof with water storage tanks for the triple absorption phase system by the accumulation of chemical energy with lithium chloride (LiCl) in summer, the energy savings would be considerable. These savings would be 77.48% compared to OP 1, and 31.47% compared to OP 2. The investment could be amortized in just over 15 years, generating an annual CO_2 emission reduction of 2190 kg.

The results on the reductions in the annual energy demand we obtained are similar to those found in previous studies for an isolated single-family house (31.85%), and somewhat lower than those obtained for an office block (36.35%), both on the Spanish Mediterranean coast. This latter difference is due to the offices being a large-scale installation with a wider and more demanding usage regime in terms of the iT and RH conditions. Solar thermal panels in an active solar system were more efficient than passive conditioning systems for both heating and cooling. In combination with the TCP panels, the annual energy demand was reduced by 69.47%, compared to a reduction of 20%–25% in the case of a greenhouse on the façade, or a reduction of 38.85% when using the basement as a passive cooling system in summer and for the damping of thermal gaps in winter.

Radiant surface conditioning systems are far superior in terms of comfort to convective systems. This research demonstrated that it is feasible to implement them in residential blocks. The periods of amortization of the investment (cost efficiency, payback time) could be considerably reduced by state subsidies justified by the benefits of significant CO_2 emission reductions, improved environmental management, and a healthier environment.

Future studies will compare energy consumption results of TCP panels applied to an office at the University of Alicante, in view of assessing their viability for the Spanish Mediterranean coast. Home automation energy consumption monitoring based on electricity and flow meters will let us know the real levels of energy consumption due to dehumidification. In this way, it will be possible to gain more accurate knowledge of the energy saved by using TCP panels and we will be able to assess their comparative viability under different climates.

References

1. Directive 2002/91/EC of the European Parliament and of the Council of 16 December 2002 on the Energy Performance of Buildings. Available online: http://eur-lex.europa.eu/legal-content/EN/TXT/?uri=celex:32002L0091 (accessed on 10 November 2017).

2. Directorate General for Energy (European Commission) European Union. Energy in Figures. Statistical Pocketbook. 2016. Available online: https://publications.europa.eu/en/publication-detail/-/publication/c3d179b2-9a82-11e6-9bca-01aa75ed71a1 (accessed on 6 November 2017).

3. Commission of the European Communities Action Plan for Energy Efficiency: Realising the Potential. Available online: http://ec.europa.eu/smart-regulation/impact/ia_carried_out/docs/ia_2006/sec_2006_1174_en.pdf (accessed on 13 November 2017).

4. Monge-Barrio, A.; Sánchez-Ostiz, A. Energy efficiency and thermal behaviour of attached sunspaces, in the residential architecture in Spain. Summer Conditions. *Energy Build.* **2015**, *108*, 244–256. [CrossRef]

5. Domínguez Amarillo, S.; León Rodríguez, Á.L.; Bustamante Rojas, P.; Sendra, J.J. Energy Intervention in the residential sector in the south of Spain: Current challenges. *Inf. Constr.* **2013**, *65*, 457–464.

6. Echarri, V.; Galiano, A.; Espinosa, A. Energy Rehabilitation of Ventilated Façades Using Phenolic Panelling at The University of Alicante Museum: Thermal Characterisation and Energy Demand. *WIT Trans. Built Environ.* **2017**, *171*, 3–15.

7. American Society of Heating, Refrigerating, and Air-Conditioning Engineers. *2010 ASHRAE Handbook: Refrigeration*; American Society of Heating, Refrigerating, and Air-Conditioning Engineers: Atlanta, GR, USA, 2010; ISBN 9781933742823.

8. Fanger, O.P. *Thermal Comfort. Analysis and Applications in Environmental Engineering*; McGraw-Hill: Copenhagen, Denmark, 1970; ISBN 8757103410.

9. De Dear, R.J.; Akimoto, T.; Arens, E.A.; Brager, G.; Candido, C.; Cheong, K.W.D.; Li, B.; Nishihara, N.; Sekhar, S.C.; Tanabe, S.; et al. Progress in thermal comfort research over the last twenty years. *Indoor Air* **2013**, *23*, 442–461. [CrossRef] [PubMed]

10. Halawa, E.; van Hoof, J. The adaptive approach to thermal comfort: A critical overview. *Energy Build.* **2012**, *51*, 101–110. [CrossRef]

11. Ministerio de Vivienda Real Decreto 314/2006, de 17 de Marzo, por el que se Aprueba el Código Técnico de la Edificación | Instituto Nacional de Seguridad e Higiene en el Trabajo (INSHT). Available online: http://www.boe.es/buscar/act.php?id=BOE-A-2006-5515 (accessed on 2 November 2017).

12. Herramienta Unificada Lider-Calener (HULC). Available online: https://www.codigotecnico.org/index.php/menu-recursos/menu-aplicaciones/282-herramientaunificada-lider-calener.html (accessed on 9 September 2017).

13. García-Romero, A.; Diarce, G. Phase Change Materials, PCMs, for thermal energy storage and their use in buildings. In *Arquit. Ecoeficiente*; Hernández, R., Irulegui, O., Aranjuelo, M., Eds.; Servicio Editorial de la UPV/ EHU: San Sebastián, Spain, 2012; Chapter 2; Volume I, pp. 129–146, ISBN 978-84-9860-688-1.

14. Hispania, U. Estudio de Viabilidad de los Sistemas: Climatización Invisible Uponor y Sistema Convencional Mediante Fan Coils 2014. Available online: https://www.uponor.es/-/media/country-specific/spain/download-centre/case-study/informe-hotel_suelo-radiante.pdf (accessed on 9 August 2017).

15. Climate WellTM 10 Design Guidelines. Available online: http://www.solarcombiplus.eu/docs/SolarCombi_ClimateWell_trainingmaterial5.pdf (accessed on 3 August 2018).

16. Stetiu, C. Energy and peak power savings potential of radiant cooling systems in US commercial buildings. *Energy Build.* **1999**, *30*, 127–138. [CrossRef]

17. *Beka Technical Information G0*; Beka Heiz-undKülmatten: Berlín, Germany, 2000.

18. Bruelisauer, M.; Chen, K.W.; Iyengar, R.; Leibundgut, H.; Li, C.; Li, M.; Mast, M.; Meggers, F.; Miller, C.; Rossi, D.; et al. BubbleZERO—Design, Construction and Operation of a Transportable Research Laboratory for Low Exergy Building System Evaluation in the Tropics. *Energies* **2013**, *6*, 4551–4571. [CrossRef]

19. Wang, Y.H. Experimental Study of Capillary Radiant Cooling System with Parameters Changing. *Appl. Mech. Mater.* **2013**, *300–301*, 1048–1053. [CrossRef]

20. Jordan, S.; Hafner, J.; Kuhn, T.E.; Legat, A.; Zbašnik-Senegačnik, M. Evaluation of Various Retrofitting Concepts of Building Envelope for Offices Equipped with Large Radiant Ceiling Panels by Dynamic Simulations. *Sustainability* **2015**, *7*, 13169–13191. [CrossRef]

21. Sala Lizarraga, J.M. Transmisión de calor en edificios. In *Arquitectura Ecoeficiente*; Servicio Editorial de la UPV/EHU: Valencia, Spain, 2012; Volume 1.

22. Mikeska, T.; Svendsen, S. Dynamic behavior of radiant cooling system based on capillary tubes in walls made of high performance concrete. *Energy Build.* **2015**, *108*, 92–100. [CrossRef]

23. Mikeska, T.; Fan, J.; Svendsen, S. Full scale measurements and CFD investigations of a wall radiant cooling system integrated in thin concrete walls. *Energy Build.* **2017**, *139*, 242–253. [CrossRef]

24. Imanari, T.; Omori, T.; Bogaki, K. Thermal comfort and energy consumption of the radiant ceiling panel system.: Comparison with the conventional all-air system. *Energy Build.* **1999**, *30*, 167–175. [CrossRef]

25. Rhee, K.-N.; Kim, K.W. A 50 year review of basic and applied research in radiant heating and cooling systems for the built environment. *Build. Environ.* **2015**, *91*, 166–190. [CrossRef]

26. Tye-Gingras, M.; Gosselin, L. Comfort and energy consumption of hydronic heating radiant ceilings and walls based on CFD analysis. *Build. Environ.* **2012**, *54*, 1–13. [CrossRef]

27. Corgnati, S.P.; Perino, M.; Fracastoro, G.V.; Nielsen, P.V. Experimental and numerical analysis of air and radiant cooling systems in offices. *Build. Environ.* **2009**, *44*, 801–806. [CrossRef]

28. Xie, D.; Wang, Y.; Wang, H.; Mo, S.; Liao, M. Numerical analysis of temperature non-uniformity and cooling capacity for capillary ceiling radiant cooling panel. *Renew. Energy* **2016**, *87*, 1154–1161. [CrossRef]

29. Seyam, S.; Huzayyin, A.; El-Batsh, H.; Nada, S. Experimental and numerical investigation of the radiant panel heating system using scale room model. *Energy Build.* **2014**, *82*, 130–141. [CrossRef]

30. Echarri, V. Thermal Ceramic Panels and Passive Systems in Mediterranean Housing: Energy Savings and Environmental Impacts. *Sustainability* **2017**, *9*, 1613. [CrossRef]

31. Echarri, V.; Galiano Garrigós, A.L.; González Avilés, Á.B. Ceramics and healthy heating and cooling systems: Thermal ceramic panels in buildings. Conditions of comfort and energy demand versus convective systems. *Inf. Constr.* **2016**, *68*, 1–14.

32. Echarri, V.; Oviedo, E.; Lázaro, V. Panel de Acondicionamiento Térmico Cerámico. Patente de nº Solicitud P201001626, 28 December 2010.

33. Dynamobel Manual de Climatización Tranquila. Available online: www.dynamobel.com (accessed on 17 January 2016).

34. Ortega, M.; Ortega, A. *Calefacción y Refrescamiento por Superficies Radiantes*; Ediciones Paraninfo, Thomson Learning: Madrid, Spain, 2001; ISBN 9788428327411.

35. Echarri, V.; Espinosa, A.; Rizo, C. Thermal Transmission through Existing Building Enclosures: Destructive Monitoring in Intermediate Layers versus Non-Destructive Monitoring with Sensors on Surfaces. *Sensors* **2017**, *17*, 2848. [CrossRef] [PubMed]

36. Echarri, V.; Espinosa Fernández, A.; Galiano Garrigós, A. Energy efficiency of flooded roofs: The University of Alicante Museum. *WIT Trans. Eng. Sci.* **2016**, *106*, 163–176.

37. Si, Q.; Zhang, X. Experimental and Numerical Study of the Radiant Induction-Unit and the Induction Radiant Air-Conditioning System. *Energies* **2017**, *10*, 26. [CrossRef]

38. Gosnell, J.; Minne, J.-P. *Radiant Cooling Systems and Applications*; The Demostration Component of the Joule-Thermie Programme; European Commission: Brussels, Belgium, 1998.

39. Dodoo, A.; Gustavsson, L.; Sathre, R. Primary energy implications of ventilation heat recovery in residential buildings. *Energy Build.* **2011**, *43*, 1566–1572. [CrossRef]

40. Peel, M.C.; Finlayson, B.L.; Mcmahon, T.A. Updated world map of the Koppen-Geiger climate classification. *Hydrol. Earth Syst. Sci.* **2007**, *11*, 1633–1644. [CrossRef]

41. Zamora García, M. Empleo de bombas de calor acopladas a intercambiadores geotérmicos en áreas costeras mediterráneas. Proyecto Geocool. Montajes e instalaciones. *Revista Técnica Sobre la Construcción e Ingeniería de las Instalaciones* **2008**, *38*, 66–72.

42. Haiwen, S.; Lin, D.; Xiangli, L.; Yingxin, Z. Quasi-dynamic energy-saving judgment of electric-driven seawater source heat pump district heating system over boiler house district heating system. *Energy Build.* **2010**, *42*, 889–895. [CrossRef]

43. Zhang, L. Hu Songtao Research on the Heat Pump System Using Seawater as Heat Source or Sink. *Build. Energy Environ.* **2006**, *25*, 34–38.

44. Kavanaugh, S.P.; Rafferty, K.D. *Ground-Source Heat Pumps: Design of Geothermal Systems for Commercial and Institutional Buildings*; ASHRAE American Society of Heating, Refrigerating and Air-Conditioning Engineers: Atlanta, GR, USA, 1997; ISBN 1883413524.

45. Rosiek, S.; Batlles, F.J. Shallow geothermal energy applied to a solar-assisted air-conditioning system in southern Spain: Two-year experience. *Appl. Energy* **2012**, *100*, 267–276. [CrossRef]

46. Moss, R.W.; Henshall, P.; Arya, F.; Shire, G.S.F.; Hyde, T.; Eames, P.C. Performance and operational effectiveness of evacuated flat plate solar collectors compared with conventional thermal, PVT and PV panels. *Appl. Energy* **2018**, *216*, 588–601. [CrossRef]

47. Prieto, C.; Rodríguez, A.; Patiño, D.; Cabeza, L.F. Thermal energy storage evaluation in direct steam generation solar plants. *Sol. Energy* **2018**, *159*, 501–509. [CrossRef]

48. Corona, B.; de la Rúa, C.; San Miguel, G. Socio-economic and environmental effects of concentrated solar power in Spain: A multiregional input output analysis. *Sol. Energy Mater. Sol. Cells* **2016**, *156*, 112–121. [CrossRef]

49. Lamnatou, C.; Notton, G.; Chemisana, D.; Cristofari, C. The environmental performance of a building-integrated solar thermal collector, based on multiple approaches and life-cycle impact assessment methodologies. *Build. Environ.* **2015**, *87*, 45–58. [CrossRef]

50. Bellos, E.; Tzivanidis, C. Optimization of a Solar-Driven Trigeneration System with Nanofluid-Based Parabolic Trough Collectors. *Energies* **2017**, *10*, 848. [CrossRef]

51. Bellos, E.; Tzivanidis, C.; Bellos, E.; Tzivanidis, C. Enhancing the Performance of Evacuated and Non-Evacuated Parabolic trough Collectors Using Twisted Tape Inserts, Perforated Plate Inserts and Internally Finned Absorber. *Energies* **2018**, *11*, 1129. [CrossRef]

52. Calise, F.; Figaj, R.; Vanoli, L.; Calise, F.; Figaj, R.D.; Vanoli, L. Energy and Economic Analysis of Energy Savings Measures in a Swimming Pool Centre by Means of Dynamic Simulations. *Energies* **2018**, *11*, 2182. [CrossRef]

53. Choudhury, B.; Saha, B.B.; Chatterjee, P.K.; Sarkar, J.P. An overview of developments in adsorption refrigeration systems towards a sustainable way of cooling. *Appl. Energy* **2013**, *104*, 554–567. [CrossRef]

54. Márquez, J.A.; Bohórquez, M.M.; Melgar, S.G. A New Metre for Cheap, Quick, Reliable and Simple Thermal Transmittance (U-Value) Measurements in Buildings. *Sensors* **2017**, *17*, 9.

55. Deconinck, A.-H.; Roels, S. Comparison of characterisation methods determining the thermal resistance of building components from onsite measurements. *Energy Build.* **2016**, *130*, 309–320. [CrossRef]

56. International Organization for Standardization ISO/TC 163/SC 1 Test and Measurement Methods ISO 9869–1:2014—Thermal Insulation—Building Elements—In-Situ Measurement of Thermal Resistance and Thermal Transmittance. Part 1: Heat Flow Meter Method. Available online: https://www.iso.org/standard /59697.html (accessed on 13 November 2017).

57. Gaspar, K.; Casals, M.; Gangolells, M. A comparison of standardized calculation methods for in situ measurements of façades U-value. *Energy Build.* **2016**, *130*, 592–599. [CrossRef]

58. Albatici, R.; Tonelli, A.; Michela, C. A comprehensive experimental approach for the validation of quantitative infrared thermography in the evaluation of building thermal transmittance. *Appl. Energy* **2015**, *141*, 218–228. [CrossRef]

59. Tinti, A.; Tarzia, A.; Passaro, A.; Angiuli, R. Thermographic analysis of polyurethane foams integrated with phase change materials designed for dynamic thermal insulation in refrigerated transport. *Appl. Therm. Eng.* **2014**, *70*, 201–210. [CrossRef]

60. Theodosiou, T.; Tsikaloudaki, K.; Kontoleon, K.; Bikas, D. Thermal bridging analysis on cladding systems for building facades. *Energy Build.* **2015**, *109*, 377–384. [CrossRef]

61. Sarbu, I.; Sebarchievici, C. Review of solar refrigeration and cooling systems. *Energy Build.* **2013**, *67*, 286–297. [CrossRef]

62. Arce, P.; Medrano, M.; Gil, A.; Oró, E.; Cabeza, L.F. Overview of thermal energy storage (TES) potential energy savings and climate change mitigation in Spain and Europe. *Appl. Energy* **2011**, *88*, 2764–2774. [CrossRef]

63. Balghouthi, M.; Chahbani, M.H.; Guizani, A. Investigation of a solar cooling installation in Tunisia. *Appl. Energy* **2012**, *98*, 138–148. [CrossRef]

64. Neila González, J.; Bedoya Frutos, C. *Técnicas Arquitectónicas y Constructivas de Acondicionamiento Ambiental*; Editorial Munilla-Lería: Madrid, Spain, 1997; ISBN 9788489150201.

65. Norma UNE-EN ISO 13790:2011. Energy Performance of Buildings. Calculation of Energy Use for Space Heating and Cooling. Available online: https://www.une.org/encuentra-tu-norma/busca-tu-norma/norm a/?c=N0048301 (accessed on 1 October 2018).

66. Dong, M.; Zhong, M.; Mo, T.-Z.; Yang, J.-Y.; Leng, Y.F.; Yang, L. Quantitative analysis on the effect of thermal bridges on energy consumption of residential buildings in hot summer and cold winter region. *J. Civ. Archit. Environ. Eng.* **2007**, *2008*, 5–8.

67. Echarri, V.; Galiano, A.; Pérez-Millán, M.I.; González-Avilés, A.B. Conditioning systems by radiant surfaces: Comparative analysis of thermal ceramic panels versus the conventional systems in a museum. *WIT Trans. Eng. Sci.* **2014**, *83*, 287–301.

68. Tahat, M.A.; Al-Hinai, H.; Probert, S.D. Performance of a low-energy-consumption house experiencing a Mediterranean climate. *Appl. Energy* **2002**, *71*, 1–13. [CrossRef]

69. Marrasso, E.; Roselli, C.; Sasso, M.; Tariello, F.; Marrasso, E.; Roselli, C.; Sasso, M.; Tariello, F. Analysis of a Hybrid Solar-Assisted Trigeneration System. *Energies* **2016**, *9*, 705. [CrossRef]

70. Saint, R.; Garnier, C.; Pomponi, F.; Currie, J.; Saint, R.M.; Garnier, C.; Pomponi, F.; Currie, J. Thermal Performance through Heat Retention in Integrated Collector-Storage Solar Water Heaters: A Review. *Energies* **2018**, *11*, 1615. [CrossRef]

71. Bataineh, K.; Taamneh, Y. Review and recent improvements of solar sorption cooling systems. *Energy Build.* **2016**, *128*, 22–37. [CrossRef]

72. Sancho, J.; Riesco, J.; Jiménez, C. Atlas de Radiación Solar en España Utilizando datos del SAF de Clima de EUMETSAT. Madrid, 2005. Available online: http://www.aemet.es/documentos/es/serviciosclimaticos/d atosclimatologicos/atlas_radiacion_solar/atlas_de_radiacion_24042012.pdf (accessed on 14 September 2018).

73. Velasco, A.; Jiménez García, S.; Guardo, A.; Fontanals, A.; Egusquiza, M. Assessment of the Use of Venetian Blinds as Solar Thermal Collectors in Double Skin Facades in Mediterranean Climates. *Energies* **2017**, *10*, 1825. [CrossRef]

74. Aroca-Delgado, R.; Pérez-Alonso, J.; Callejón-Ferre, Á.J.; Velázquez-Martí, B. Compatibility between Crops and Solar Panels: An Overview from Shading Systems. *Sustainability* **2018**, *10*, 743. [CrossRef]

75. Valančius, R.; Jurelionis, A.; Jonynas, R.; Katinas, V.; Perednis, E.; Valančius, R.; Jurelionis, A.; Jonynas, R.; Katinas, V.; Perednis, E. Analysis of Medium-Scale Solar Thermal Systems and Their Potential in Lithuania. *Energies* **2015**, *8*, 5725–5737. [CrossRef]

76. Erdenedavaa, P.; Rosato, A.; Adiyabat, A.; Akisawa, A.; Sibilio, S.; Ciervo, A. Model Analysis of Solar Thermal System with the Effect of Dust Deposition on the Collectors. *Energies* **2018**, *11*, 1795. [CrossRef]

77. Budea, S. Solar Air Collectors for Space Heating and Ventilation Applications—Performance and Case Studies under Romanian Climatic Conditions. *Energies* **2014**, *7*, 3781–3792. [CrossRef]

78. Oregi, X.; Hernandez, P.; Gazulla, C.; Isasa, M. Integrating Simplified and Full Life Cycle Approaches in Decision Making for Building Energy Refurbishment: Benefits and Barriers. *Buildings* **2015**, *5*, 354–380. [CrossRef]

79. ELCD Database. Available online: www.eplca.jcr.ec.europa.eu/ELCD3/index.xhtml;jsessionid=9FC03F3B6A0A5F8252F667E462DF467C (accessed on 27 August 2018).

80. IDAE. Informe de Precios Energéticos Regulados. Julio 2017. Available online: http://www.idae.es/sites/default/files/estudios_informes_y_estadisticas/tarifas_reguladas_julio_2017.pdf (accessed on 3 September 2018).

81. Mahmud, M.; Huda, N.; Farjana, S.; Lang, C.; Mahmud, M.A.P.; Huda, N.; Farjana, S.H.; Lang, C. Environmental Impacts of Solar-Photovoltaic and Solar-Thermal Systems with Life-Cycle Assessment. *Energies* **2018**, *11*, 2346. [CrossRef]